Numerical Multiphase PTA

Vincent Artus - Gérard Pellissier - Olivier Allain

1. Introduction

In 2004-2005, KAPPA developed a multiphase option in Saphir NL. This option allowed 2-phase flow without exchange between the phases (eg water injection in dead oil, or gas) and complex 3-phase flow with phase exchanges, for black-oil or condensate. In all those situations, it was soon realized that multiphase simulations could exhibit large oscillations on the loglog derivative. In the case of water injection, we were able to damp these oscillations through the use of pseudo-kr corrections, but no 'easy' solution was found for black-oil or condensate. As a consequence, a complete 3-phase option was not released, and Saphir NL was limited to two-phase PVT including water.

With the sector model option of Rubis v4.12, 3-phase simulations can *de facto* be run in Saphir NL, albeit through a tortuous path. It was thus decided to make the full multiphase option directly accessible in Saphir NL during the course of the v4.20 upgrades, after a detailed investigation of the nature of the oscillations, and the possible solutions to damp them. This document summarizes the work undertaken; its reading is highly recommended before running any multiphase Saphir NL cases. It is important to note that the problems described here go unnoticed in numerical simulation, while they are exemplified in PTA by the use of the pressure derivative, and the focus on short time scale.

Approximately a hundred numerical simulations have been run for this study, covering various multiphase contexts across a wide range of depletion levels. Although no generic description is possible because visible effects are strongly dependent on the simulation context (PVT, KrPc, etc…), most of the possible situations are covered by the examples in this document.

Four main cases are presented:

- Case 1 (section 2.1): water injection in an oil reservoir. Illustration of the development of oscillations while flooding; the origin of oscillations is explained in section 2.2.
- Case 2 (section 2.4): complex history of water injection into an oil reservoir. Validation of the numerical model against the analytical results.
- Case 3 (section 3.1): depletion into a black-oil reservoir. The origin of oscillations is analyzed in section 3.2; section 3.3 is dedicated to the interpretation of the results.
- Case 4 (section 4.1): depletion of a condensate gas reservoir.
  The results are interpreted in section 4.2.

Yellow sections of this document are not strictly required for a global comprehension of the origin of oscillations with multiphase transient simulations. However, they provide interesting material for a deeper analysis of the complexity of the various physical mechanisms involved with multiphase processes.

2. Water or gas injection

We start with the analysis of injection of one phase into another, without mass transfer between the two phases. Although we illustrate the effects based on the results of simulations of water injection into dead oil, the main features described below remain valid for other injection schemes (e.g. water injection into gas, gas injection, etc...).

Two test cases are presented. Case 1 illustrates and explains the development of oscillations, while Case 2 is a validation of the numerical model against analytical predictions.

2.1. Test Case 1

Test description

We consider a rectangular reservoir of dimensions 10,000×10,000 ft², with thickness 100 ft. The injection well is located at the center of the reservoir. The formation compressibility is cf=3e-6 psi^{-1}, the permeability is k=1000 mD, and the porosity is ϕ=0.2. The reservoir initially contains dead-oil, with constant properties (μo = 0.3 cp, Bo=1). The initial water saturation in the reservoir is Swi=0.2. Water is injected for 10,000 hr at constant rate Qw=10,000 stb/D, followed by a 10,000 hr fall-off. Water is also characterized by constant properties (μw = 0.3cp, Bw=1). Equal viscosities between oil and water have been chosen so that the mobility effects are only due to the choice of relative permeability curves. Relative permeabilities have the following properties:

- Kromax = 0.8; Krwmax = 0.5; Swr = 0.2; Sor = 0.25
- The curve shape is a power curve (Corey type). 3 values of the Corey exponent have been tested: 1 (called test "Corey 1"), 2 ("Corey 2") and 3 ("Corey 3"), in order to show the influence of the non-linearity of Kr curves on oscillations.

Results

During the injection phase, the pressure derivative exhibits oscillations on the loglog plot. The level of these oscillations increases with the non-linearity of the relative permeability curves (Figure 1). This can be related to an increase of the mobility contrasts with the non-linearity of the curves.

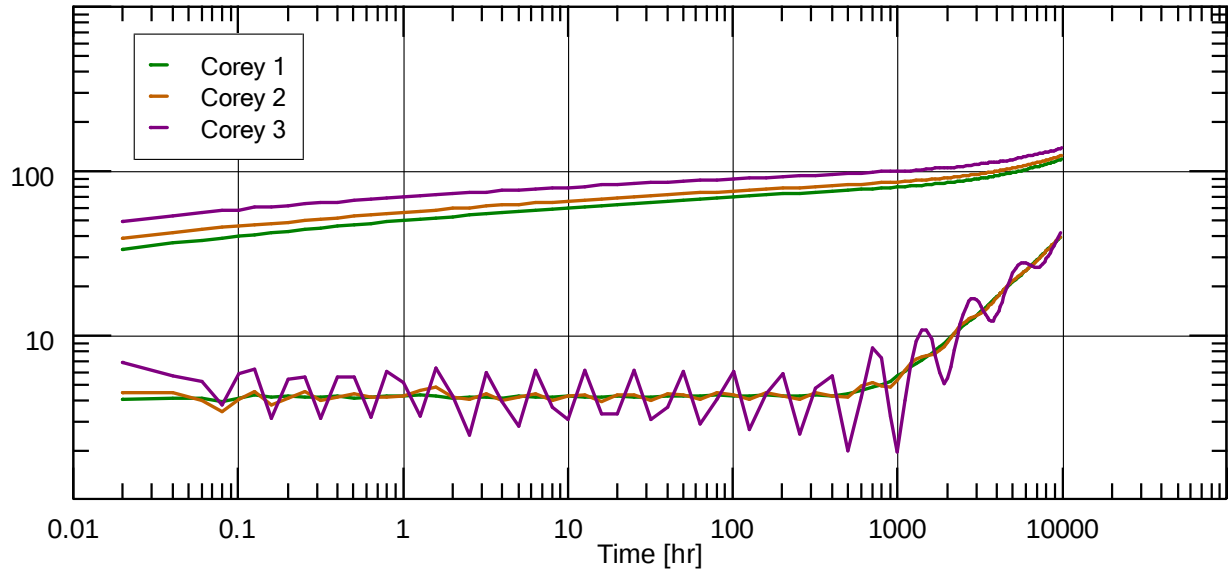

Figure 1: Water injection for 3 values of the exponent of the relative permeability curves

Looking at the evolution of the water saturation field during the injection, we see that every oscillation on the loglog plot corresponds to the invasion of a new ring of cells by the water bank (Figure 2). The higher the mobility contrast between the water bank and the initial oil, the larger the resulting oscillations.

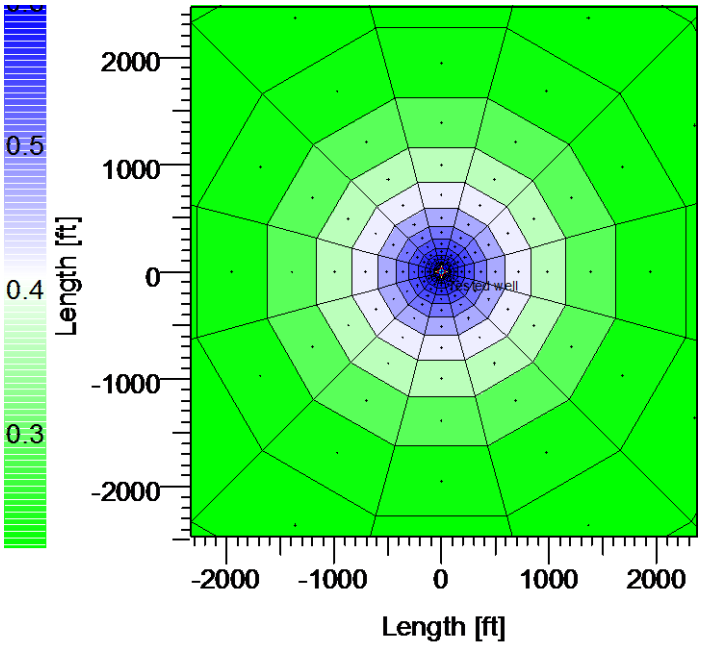

Figure 2: Water saturation map around the well at the end of the injection period

Although the level of the oscillations can be spectacular for strong mobility contrasts (e.g. Figure 1 for Corey 3 curves), it can be greatly reduced by refining the simulation grid. Figure 3 compares the results obtained using a gridding progression ratio of 1.4 with those obtained using ratios of 1.2 and 1.1, in the case of very non-linear curves (Corey 3). It is worth noticing that for weaker contrasts (Corey 1 and 2), the oscillations almost completely disappear with a gridding progression ratio of 1.2.

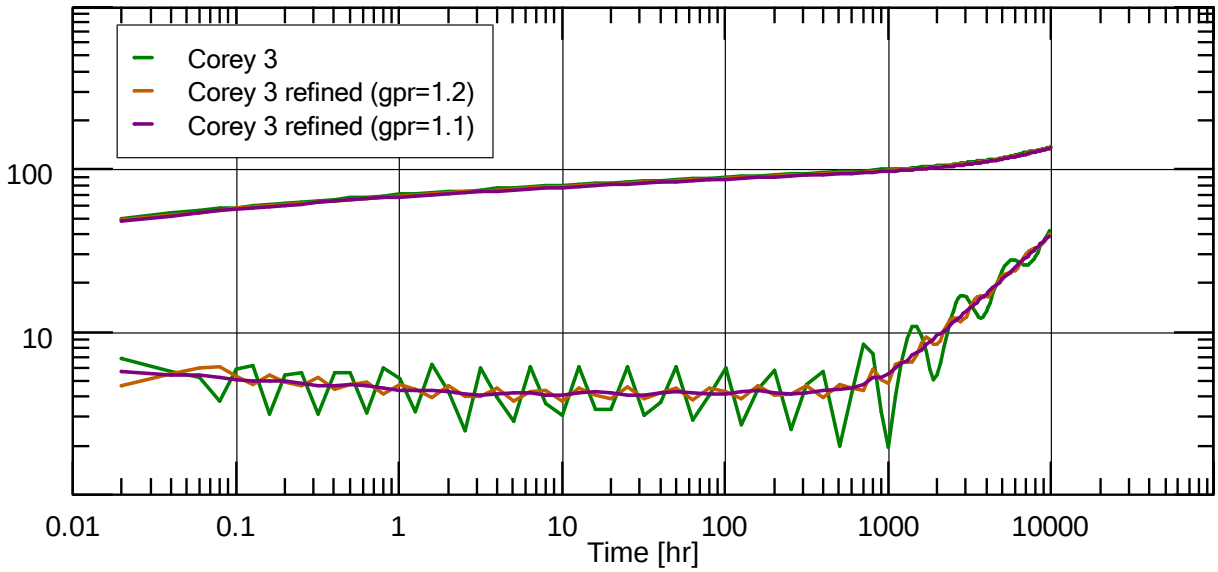

Figure 3: Effect of grid refinement on oscillations (gpr = gridding progression ratio)

On the right side of Figure 3, one can see that reducing the cell size increases the frequency of oscillations, but also reduces their amplitude. This is explained in the next section.

2.2. Origin of oscillations

Let us consider a 1D displacement of oil by water, water being injected at constant rate. Both fluids are assumed incompressible. From viscosity values and kr curves, the oil, water and total mobility curves can be derived:

$$\lambda_o(S_w) = \frac{\mu_o}{k_{ro}(S_w)} \qquad \lambda_w(S_w) = \frac{\mu_w}{k_{rw}(S_w)}$$

$$\lambda_t(S_w) = \lambda_o(S_w) + \lambda_w(S_w)$$

Such curves are presented on Figure 4. Note that for the sake of illustration in all the figures below, we used the same viscosity values as in test case 1, with the "Corey 2" relative permeability curves. It is important to notice that due to the non-linearity of the relative permeability curves, the total mobility curve is also non-linear. Indeed, as shown on figure 4, the total mobility starts to decrease when the water saturation increases from S_{wr}, before increasing again as S_w approaches $(1-S_{or})$.

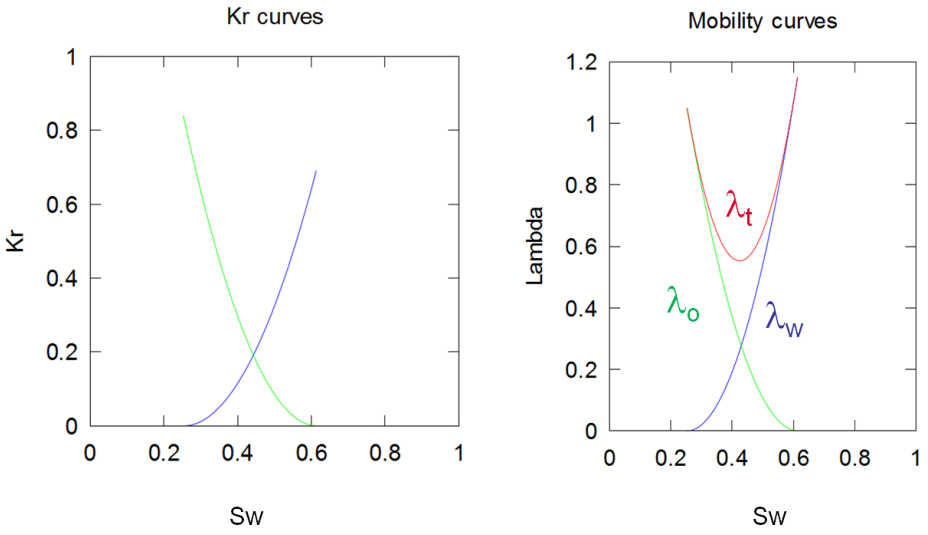

Figure 4: Relative permeability and mobility curves

Let us know consider the classical Buckley-Leverett model (Buckley and Leverett, 1942, Marle, 1981) to further investigate the problem. With this model, the 1D, incompressible displacement in the absence of capillary pressure and gravity can be described with the following hyperbolic equation:

$$\frac{u}{\phi}\left(\frac{df}{dS_w}\frac{\partial S_w}{\partial x}\right)+\frac{\partial S_w}{\partial t}=0$$

Above, u is the total velocity, ϕ is the porosity, and f is the water fractional flow, defined as:

$$f = \frac{u_w}{u}$$

The Buckley-Leverett analysis shows that the fractional flow actually depends on the water saturation only, and can be expressed:

$$f(S_w) = \frac{\lambda_w}{\lambda_t}$$

Such a fractional flow curve is presented on the left side of Figure 5. Using the method of characteristics to solve the hyperbolic equation, it can be shown that each saturation plane travels at its own, constant speed:

$$V(S_w) = \frac{df(S_w)}{dS_w}$$

This leads to the velocity profile shown on the right side of Figure 5. Because low saturation planes travel slowly compared to some higher saturation planes, a saturation front appears. The value of the front saturation Sf can be deduced from the fractional flow curve through Welge's tangency (left of Figure 5), as developed in Marle, 1981.

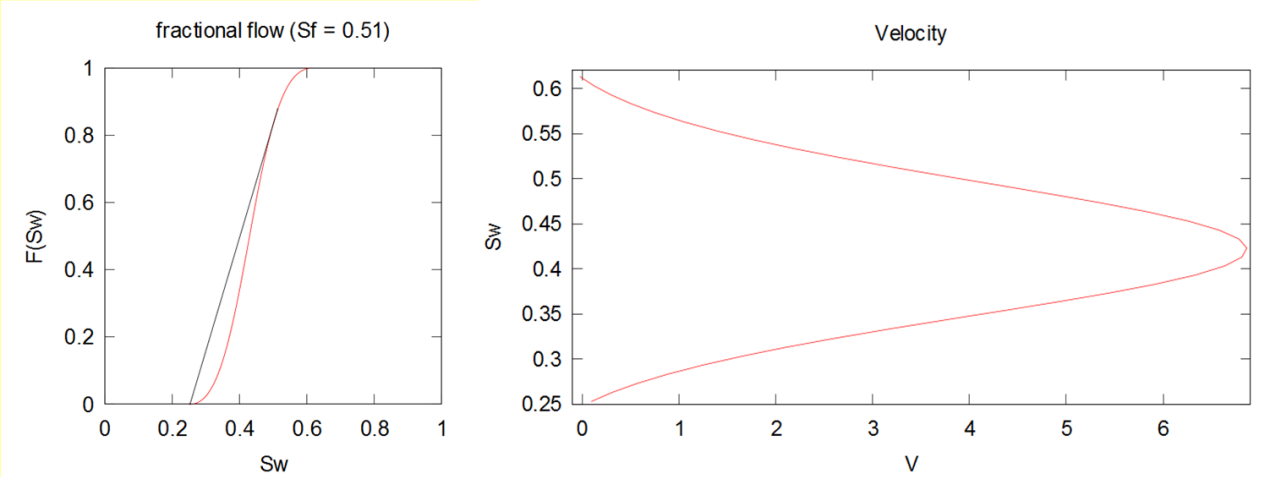

Figure 5: Fractional flow and velocity profile corresponding to the curves of Figure 4.

From the front saturation value and from the velocity profile, it is easy to derive the evolution of the saturation profiles during the 1D flooding of the porous medium. The left side of Figure 6 gives such profiles for three different times.

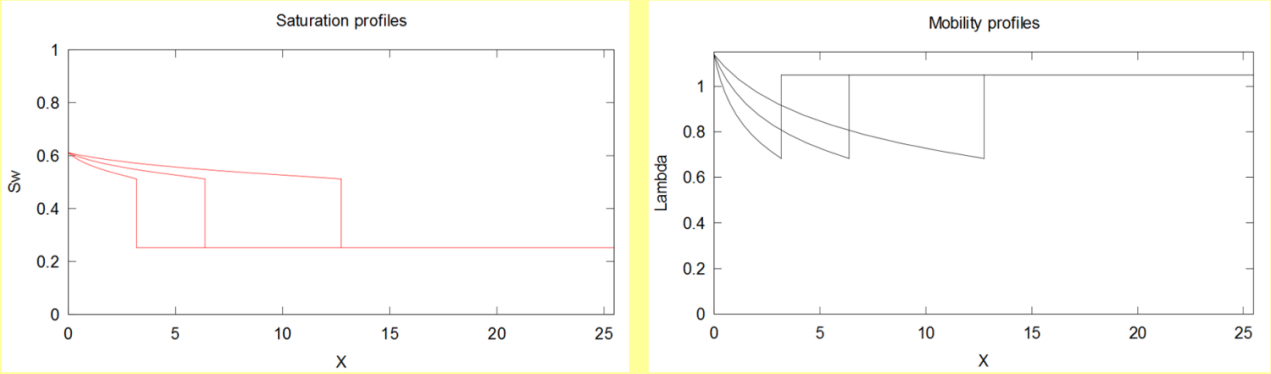

Figure 6: Saturation and mobility profiles at 3 different times, corresponding to curves of Figure 4

From any water saturation profile and mobility curves, one can also derive the corresponding total mobility profile (right side of Figure 6).

Across the saturation shock, a total mobility shock is also experienced. Let us call *r* the mobility ratio across the front:

$$r = \lambda_t(S_f) / \lambda_t(S_{wr})$$

This mobility ratio is responsible for the stability of the displacement process. If the injected fluid is less mobile *at the front* than the displaced fluid, the ratio $r < 1$ is said favorable: in this case, the displacement is stable and viscous fingering cannot develop. If $r > 1$, the ratio is unfavorable: viscous fingering can develop and reduce the sweep efficiency. It is interesting to notice that while the end-point mobility ratio seems unfavorable in Figure 6, the non-linearity of relative permeability curves leads to a favorable mobility ratio at the front. As a consequence, the overall displacement is stable. Stable displacements can hence arise even if the viscosity of the injected fluid is lower than the viscosity of the fluid in place (King and Dunayevsky, 1989).

Note that in Test Case 1, tuning the Corey exponent between 1 and 3 was a way to tune the mobility contrast across the saturation front, and trigger larger oscillations.

Let us now consider a well-developed 1D injection profile. We focus on a region close to the front, and assume that upstream of this front (located at x) the evolution of the saturation is negligible (Figure 7).

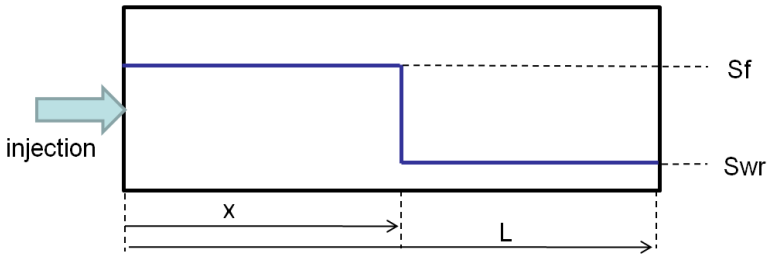

Figure 7: 1D displacement with the continuous model

In the continuous model (Figure 7), the pressure drop in the medium can be expressed as:

$$\Delta P = C \cdot \left(\frac{x}{\lambda_t(S_f)} + \frac{L - x}{\lambda_t(S_{wr})} \right)$$

Above, C is a constant that depends on the injection rate, the flooded section and the permeability. From this equation, we see that the pressure drop across the distance L is a continuous linear function of the position of the front.

Let us now discretize this model by introducing N cells in the problem (Figure 8).

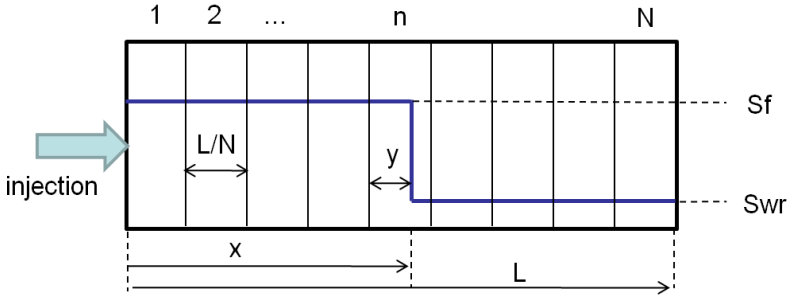

Figure 8: 1D displacement with the discrete model

In the discretized model, the position of the front within a cell is not accessible, and only the average saturation in the front cell $\overline{S_w}$ is used. The pressure drop becomes:

$$\Delta P = C.\left[\frac{(n-1)}{\lambda_t(S_f)} + \frac{1}{\lambda_t(\overline{S_w})} + \frac{(N-n)}{\lambda_t(S_{wr})}\right] \qquad \text{(Eq A)}$$

$\overline{S_w}$ can be expressed in function of the position of the front as:

$$\overline{S_w} = \frac{S_f \cdot y(x) + S_{wr} \cdot (L/N - y(x))}{L/N} \qquad \text{(Eq B)}$$

Obviously, $\overline{S_w}$ is still a linear function of x. However, the total mobility $\lambda_t(\overline{S_w})$ can be very non-linear, as shown previously on Figure 4. This explains the development of oscillations.

On Figure 9, the expression for the pressure drop in the discretized model has been solved as a function of the position of the front (Eq A and Eq B with arbitrary values L=1 and C=1), for various discretization levels N. Each oscillation corresponds to the invasion of a new cell during the displacement.

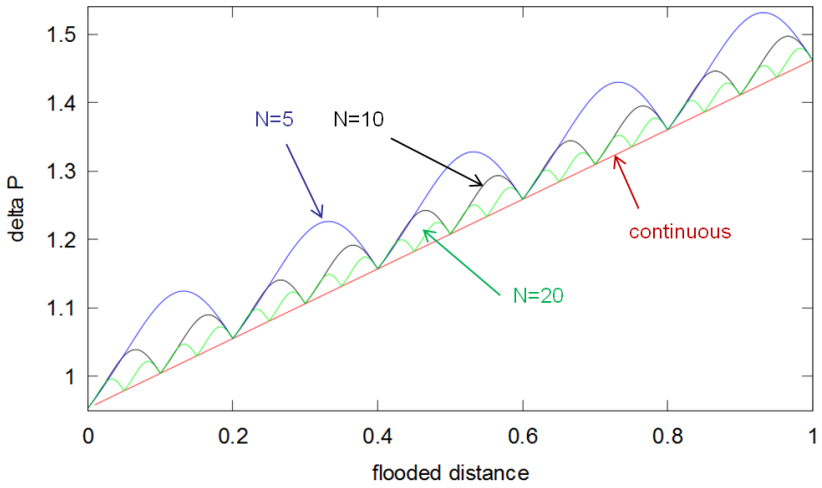

Figure 9: Oscillations obtained with the discrete model, for various discretization levels

From this model, we see that increasing the number of cells reduces the amplitude of the oscillations and increases their frequency, as was observed with Test Case 1.

2.3. Pseudo-relative permeabilities

Pseudo-relative permeabilities were originally developed to reduce the numerical dispersion during multiphase simulations (Kyte and Berry, 1968). Later, they were also used for numerical upscaling with limited success, as reviewed by Barker and Thibeau, 1996. In Ecrin, the idea was to develop pseudo-Kr curves in order to approach the continuous model and decrease the level of oscillations. Main features of these pseudos should be:

- Linear total mobility versus S_w
- Null $Kr(S_w)$ while $S_w<S_f$

The implementation of the pseudo-functions is a complex task, because the resulting curves must be continuous and the correction should apply only in cells where the front is present. As shown on Figure 10, the released solution significantly decreases the amplitude of oscillations. When used in conjunction with grid refinement, the pseudo-Kr correction can give very satisfying results.

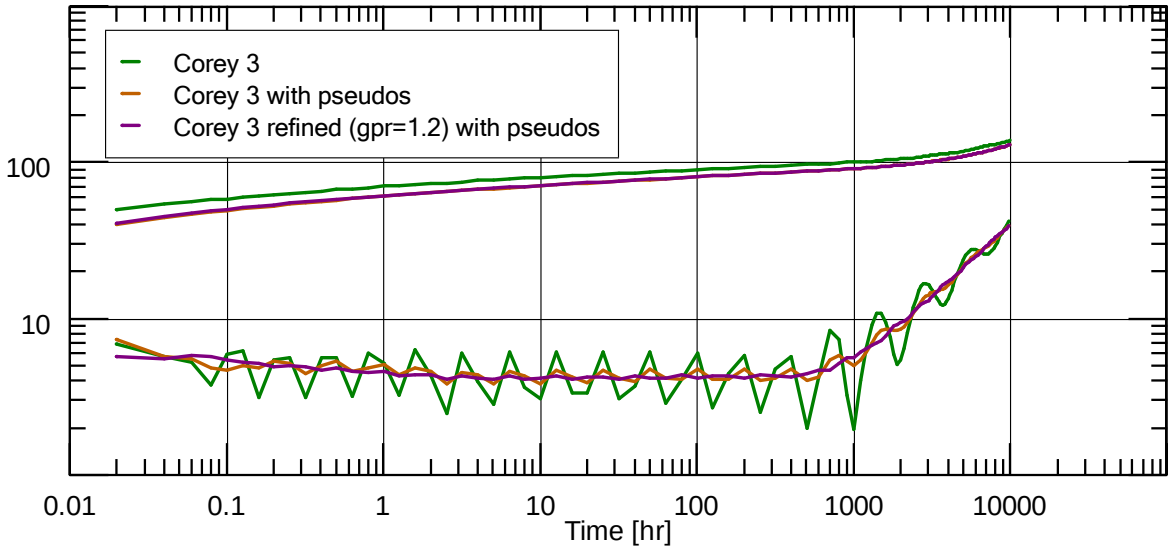

Figure 10: Oscillations damped by Pseudo-Kr and grid refinement

2.4. Test Case 2 – Interpretation of the LogLog plot

The objective of this section is to analyze the loglog plot, and to validate our numerical results against analytical models. An injection test has been simulated, based on the case from Levitan, 2002.

Test description

The reservoir is infinite (in fact, we simulate a circle with R=40,000ft) with thickness h=100ft. The porosity is Φ = 0.20 and the permeability is k = 1000 md. The rock compressibility is cr=5e-6 psi-1. The initial pressure of the reservoir is Pi = 5000 psi.
The well is localized at the center, with rw=0.357 ft. No wellbore storage is considered, in order to show the early time behavior.
The initial fluid is oil, with constant properties co = 9e-6 psi-1 and μo = 0.3 cp.
The injected fluid is water, also with constant properties cw = 3e-6 psi-1 and μw = 0.25 cp.
Finally, Kr curves are power laws with exponent 2, and:

- Swr = 0.20, Sorw = 0.25
- Krw(1-Sor) = 0.20, Krow(Swr) = 0.80

We consider the following history (Table 1), which allows analyzing 3 different positions of the water bank during fall-offs:

	Duration (hr)	Rate (stb/d)
Injection 1	1	-10,000
Buildup 1	9	0
Injection 2	10	-10,000
Buildup 2	90	0
Injection 3	100	-10,000
Buildup 3	900	0

Table 1: Injection history for Test Case 2

Results

Figure 11 presents the 3 simulated injection phases. On this figure, the data sets with markers correspond to the results obtained with the correction based on pseudo-kr curves, while the solid lines are the uncorrected simulations. We see that although strong oscillations were visible with the standard model, they are almost completely damped using the correction.

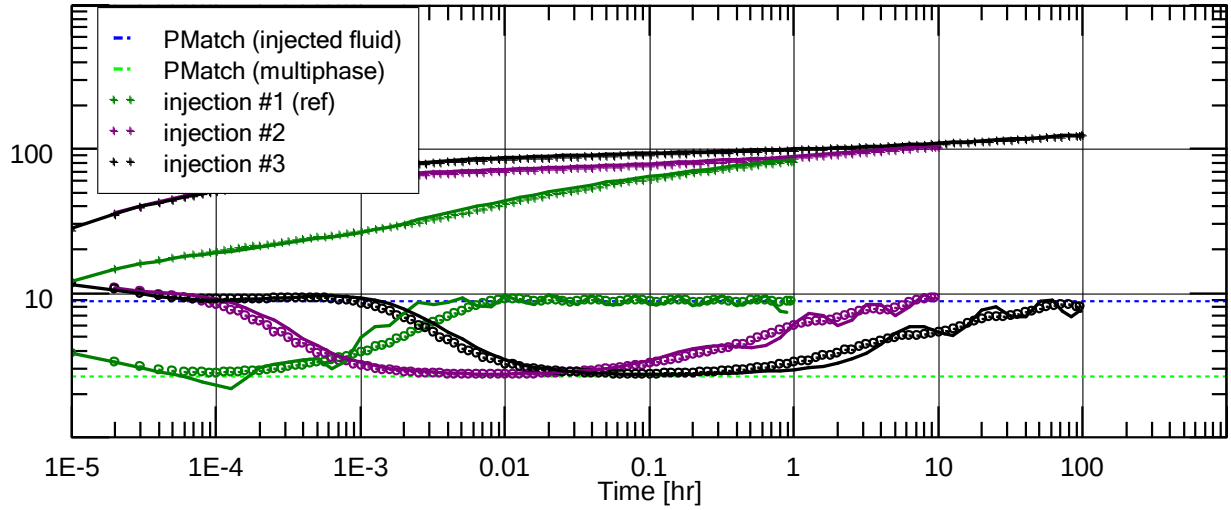

Figure 11: 3 injection curves for Test Case 2. Comparison between standard results (solid lines) and the correction based on pseudo-kr curves (markers)

Let us call λo the mobility in the original reservoir, and λw the mobility in the water invaded zone, where we assume that $Sw = 1 - Sorw$. From the viscosity values and the relative permeability data, we get:

- λo = 0.8 / 0.3
- λw = 0.2 / 0.25
- $\lambda w / \lambda o$ = 0.3

The 3 injection derivatives in figure 11 show common behavior. While the pressure investigation progresses in the reservoir, each derivative can exhibit up to 3 parts, corresponding to three successive values of the mobility: λw, λo, λw. Obviously, the first part does not appear during the first injection, because no water bank is present at the beginning. Also, the last part does not appear if the injection duration is not sufficient.

Figure 12 represents the obtained results for the 3 fall-off phases. The derivatives have 2 parts, corresponding first to λw, then to λo. The last part does not appear if the falloff duration is not sufficient.

In all cases, the first period corresponds to the nearby region, with water mobility, and the second period to the original fluid, with oil mobility. We see that the injection curve differs from the falloff curve by exhibiting a third period at the water mobility level. This corresponds to a period of predominant water displacement, and the curve shows the increase of overall pressure drop due to the extension of the water zone. Without the correction based on pseudo-kr curves, the original oscillations occur during this period, while the water front progresses from one ring of cells to another.

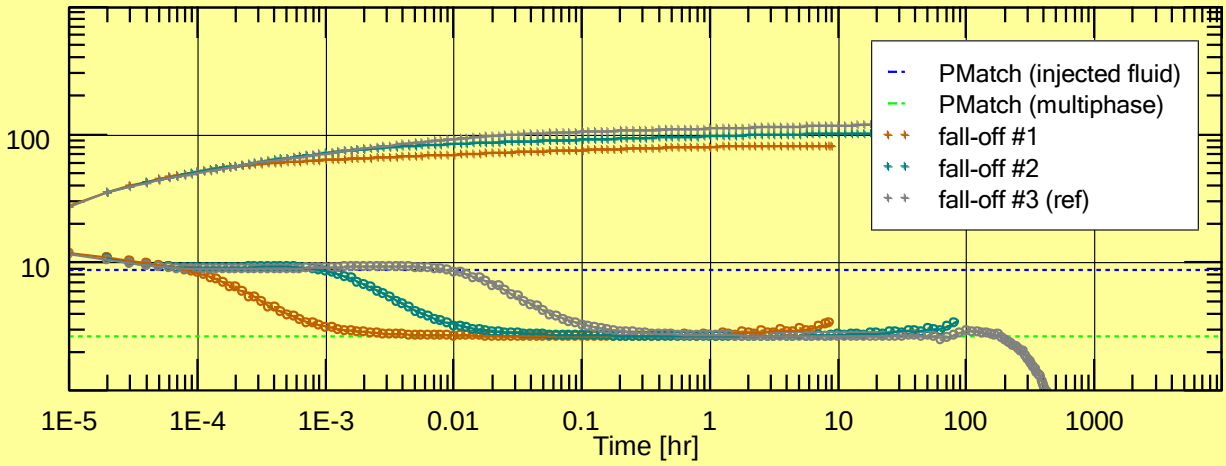

Figure 12: Fall-off curves for Test Case 2.

Comparison with analytical model

In order to justify the classical analytical interpretation, equivalent analytical simulations have been performed using a single-phase, radial composite model. The composite radius ri is computed by assuming a sharp front of injected water from *Swr* to (*1–Sorw*). This leads to three models, with radius ri=8.2, ri=27.3 and ri=86.7 ft.
From the mobility ratio, the values *μ,* M and D are computed:

- The viscosity of the equivalent fluid close from well is $\mu = \mu w / krw$ = 1.25 cp
- M = D = $(\lambda w / \lambda o)$ =0.3

The superposition of the different curves (figures 13, 14 and 15) shows a very good agreement between the numerical and the analytical models. Note that on figure 15, the late-time discrepancy on the effective boundary position is linked to existing connate water saturation in the numerical model, and could be easily corrected.

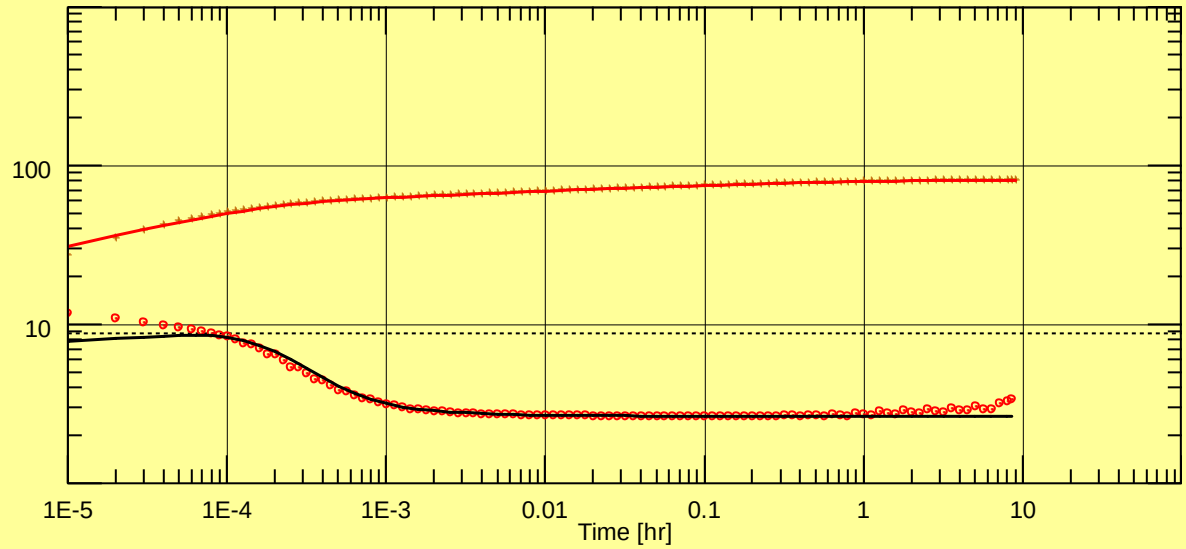

Figure 13: Analytical (solid line, ri=8.2ft) and numerical (markers)

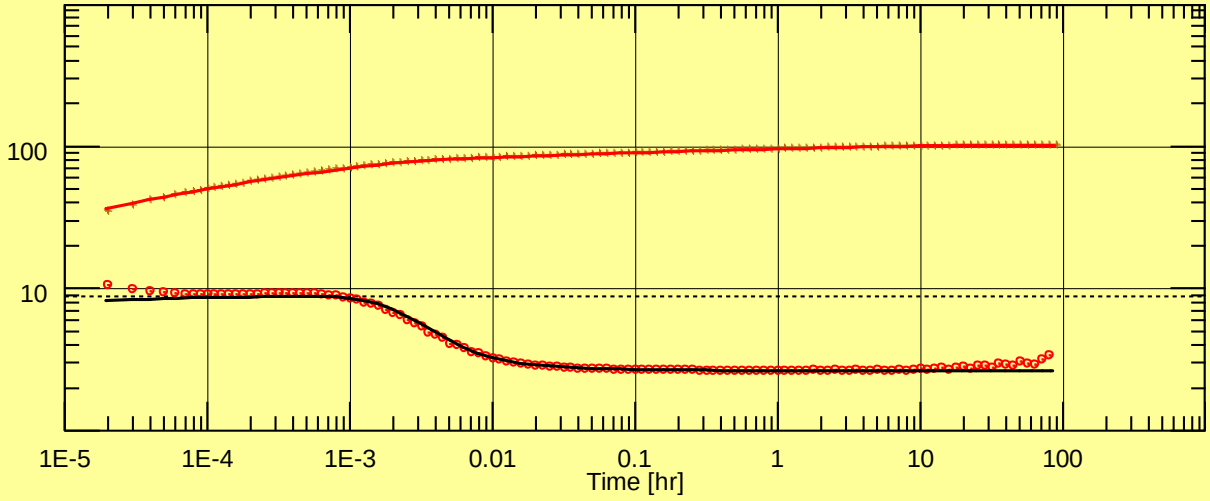

Figure 14: Analytical (solid line, ri=27.3ft) and numerical (markers)

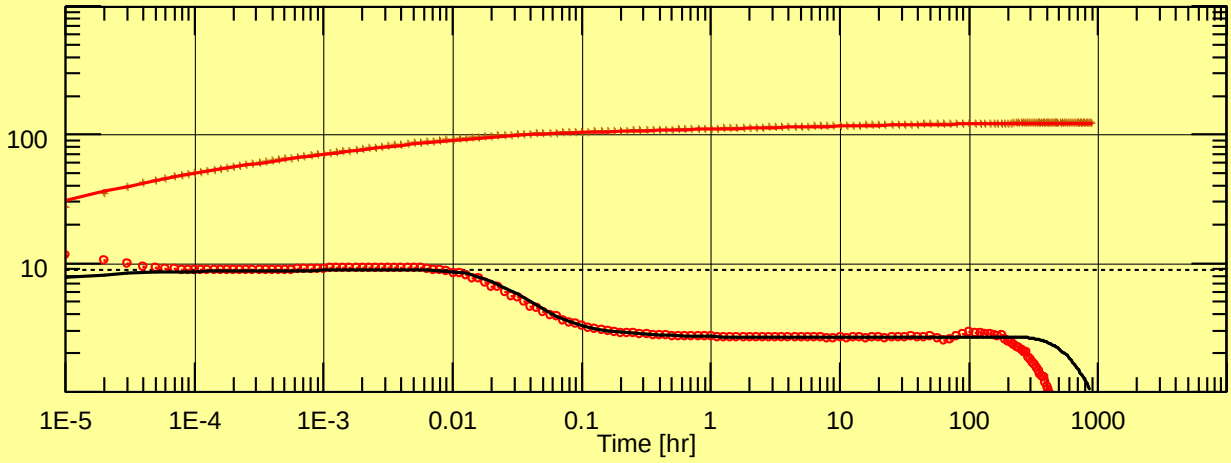

Figure 15: Analytical (solid line, ri=86.7ft) and numerical (markers)

The classical interpretation can hence provide 3 results from the derivative curve:
- The initial and water mobilities.
- The injection radius

Let us further analyze Figure 14, which shows the analytical run for a composite radius of 27.3 ft, equivalent to the cumulative injection after 11 h. Fall-off 2 shows the same behavior as the standard case:
- A first transient period can be seen, where the mobility corresponds to the water zone. In the analytical case, the mobility was calculated assuming a maximum invasion of water, at Sw = 1 – Sorw. In fact, the water saturation upstream of the front progressively varies from the Buckley-Leverett frontal saturation (Swf) to this maximum value.
- The last transient period corresponds to the mobility of the original oil zone, with initial water saturation Swi.

This comparison validates the interpretation in the two-phase model of the fall-off curve.

Although not clear here, in some cases (usually with weak mobility contrasts) one may notice that the transition period is smoother in the numerical model than in the analytical prediction. This indicates that the saturation profile sharpness of the Buckley-Leverett model is not respected, as it is in the composite analytical model. This is due to some numerical dispersion, and can be corrected using a finer simulation grid.

One can also notice that the 3 fall-off derivative curves begin to show small oscillations at late times (figures 13 and 14). These oscillations are different in nature from the previously observed ones (i.e. when the front was moving), and are due to numerical precision. This can be explained by recalling that the numerical mechanism is an iterative calculation which stops when a given convergence criterion is reached (here, a local material balance error). This implies pressure results are erratic inside a very small interval, but when the pressure variation of a time step reaches the same order of magnitude - as it is the case when the pressure completely stabilizes in the reservoir - the derivative starts to reflect this erratic behavior. This is not a significant problem, since the pressure variation itself is negligible in this period, and the length of the fall-off periods does not correspond to real cases. Note that in any case, these oscillations can be completely damped by increasing the numerical precision (i.e. by reducing the numerical mass balance error criterion in the numerical settings).

2.5. Conclusions for injection

The injection of water into an oil or gas reservoir (without mass transfer between the phases) can be simulated in transient mode using the numerical model in Saphir NL, with some specific observable behavior:

- The fall-off and injection periods exhibit a first part representative of the in place water mobility, which can be hidden by the storage effect. This corresponds to water saturation between the Buckley-Leverett front saturation and the maximum water saturation: 1-*Sorw*.
- The fall-off and injection periods exhibit a second part representative of the initial in place fluid mobility, at the connate water saturation.
- The injection period exhibits a third part representative of a mobility coming back to the level of the first part.
- The injection period is subject to oscillations due to the discretized nature of the model.
- The oscillation level increases with low mobility ratio (gas or light oil), or with large cells in the radial flow direction, and with the non-linearity of the total mobility curve. The oscillation level can be reduced by reducing the radial cell size with the gridding progression ratio, and by using a correction based on pseudo-relative permeability curves. This correction is automatically activated by default in Ecrin, in the case of water injection.

3. Black-oil production

We now analyze multiphase effects in the case of black-oil production. In this situation, mass transfer exists between the oil and the gas phases, as the light component can vaporize during depletion.

3.1. Test Case 3

Test description

The reservoir is circular, with a central production well. No water phase is considered. The initial pressure is Pi=5,000 psi. The porosity is Φ = 0.20 and the rock compressibility is cr=3e-6 psi^{-1}.
The oil phase is defined using the "saturated oil" option, with T=212 °F and GOR = 1520 scf/stb. This gives Pb=4500 psi. All other data are kept at their default values. The resulting data at bubble point are Bo=1.863, μo=0.226 cp.
The relative permeability curves are of power-law type with exponent 2, using Sorg =0.25, Sgr=0.05, Krogmax=0.8 and Krgomax=0.5.

The production history is:
- Production: duration 10,000 hr, rates Qo=10,000 stb/D and Qg=15,200 Mscf/D, giving a total constraint rate Qt=10,000 stb/D.
- Build-up: duration 10,000 hr.

In order to investigate different levels of depletion, we ran more than 30 simulations on this case, varying both the reservoir radius R (from 5,000 ft to 50,000 ft) and the reservoir permeability k (from 50 mD to 200 mD).

Results

Figure 16 shows the results for limited depletion, using R=50,000 ft and k=200 mD. In this case, the bubble point pressure is reached around the well after 30 hr production, leading to the apparition of gas in the system. As the pressure continues to drop down, the gas zone expands further away from the well, leading to oscillations. Each oscillation can be related to the apparition of gas in a new ring of cells around the well (Figure 17).

As in the case of water injection, oscillations can be explained by the progression of a saturation shock in the medium, although the physical process is different here, because the gas appears locally by depletion below the bubble point. Again, reducing the gridding progression ratio increases the frequency of oscillations but reduces their magnitude (Figure 16).

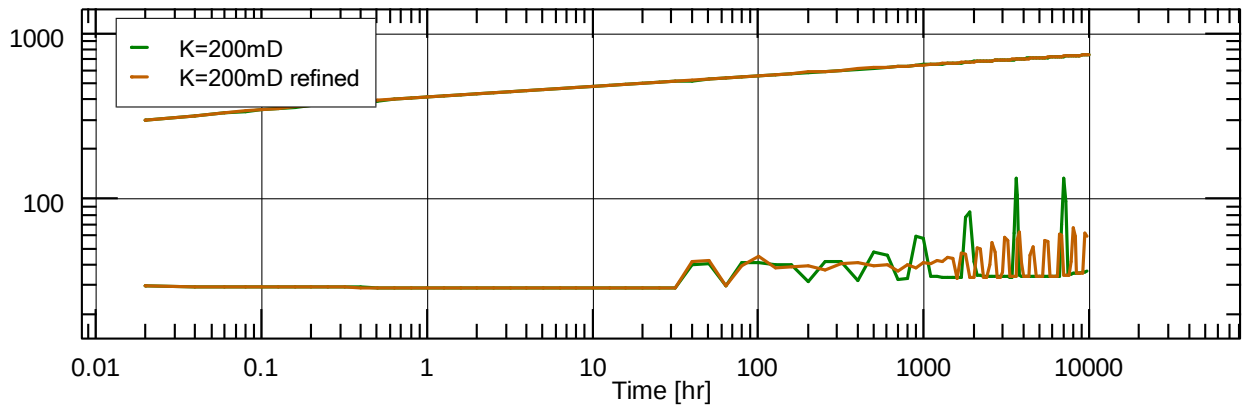

Figure 16: Effect of the discretization during production period (R=50,000 ft, k=200 mD)

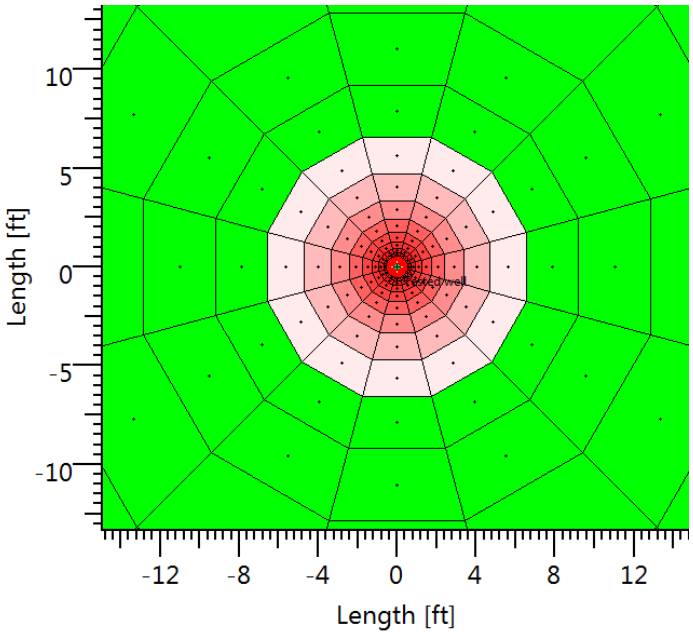

Figure 17: Gas saturation map at the end of the production period (R=50,000 ft, k=200 mD)

When the depletion is larger, as shown on Figure 18, the bubble point is reached immediately. In this case, a wider gas zone appears from the first time step and continues its expansion during the production phase. As a consequence, oscillations can be seen from the beginning on the loglog derivative. Again, reducing the gridding progression ratio clearly reduces the oscillations level.

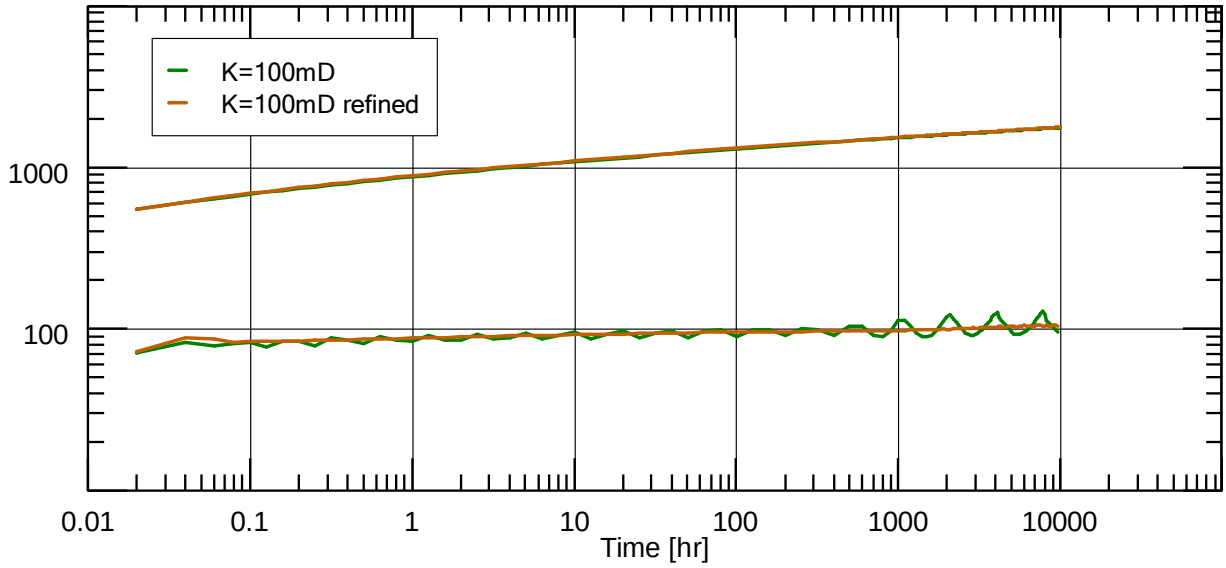

Figure 18: Effect of the discretization during production period (R=50,000 ft, k=100 mD)

3.2. Analysis of the sources of oscillations

The development of oscillations during production of black oil is a more complex process than in the case of water injection. However, it can still be related to the discretization in presence of a moving saturation front.

Let us consider a simple continuous model, using a 1-D pressure profile (Figure 19). From this profile, the corresponding pseudo-permanent saturation profile can be deduced: it is such that the flowing composition is constant everywhere, i.e. CFout=CFin on Figure 19.

Note that while the flowing composition is uniform in this model, the local compositions and saturations are not uniform.

When the pressure profile evolves slowly due to depletion, the saturation profile evolves accordingly in order to stabilize and ensure constant flowing compositions. Note also that the gas saturation profile exhibits a strong discontinuity while P decreases below Pb.

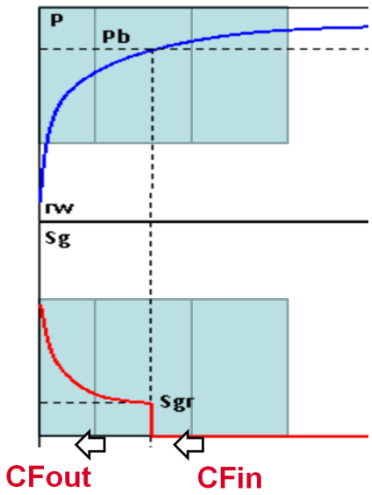

Figure 19

Although not clear on this Figure, it is interesting to point out that this simplified model leads to a saturation profile giving higher gas saturation values for a given P<Pb, compared to the saturations predicted by constant mass depletion of the original oil at the same pressure P. This point was confirmed by the results of our simulations, and will be useful further in the document, when we analyze the evolution of the GOR and the evolution of saturation maps during build-ups.

Let us now discretize our model, and focus on a cell where the saturation front is present. This front cell was initially undersaturated, and at a given time, its pressure *P* becomes lower than the entering oil saturation pressure *Pb*. The oil entering into this cell during a time step flashes and gives a free gas quantity, which is unmovable as long as the gas saturation is below the critical saturation *Sgr*. In this case, the produced fluid is no more the injected fluid: it is the saturated oil of the cell, eventually completed by an insufficient quantity of gas. As a consequence, this introduces a transient behavior, until the saturation value corresponding to the constant flowing composition is reached. This process occurs each time the gas front appears in a new cell, explaining the development of pressure derivative oscillations.

Understanding this phenomenon, it is suspected that the value of the residual saturation may have a strong influence on these oscillations. This is confirmed by examining the results of Figure 20.

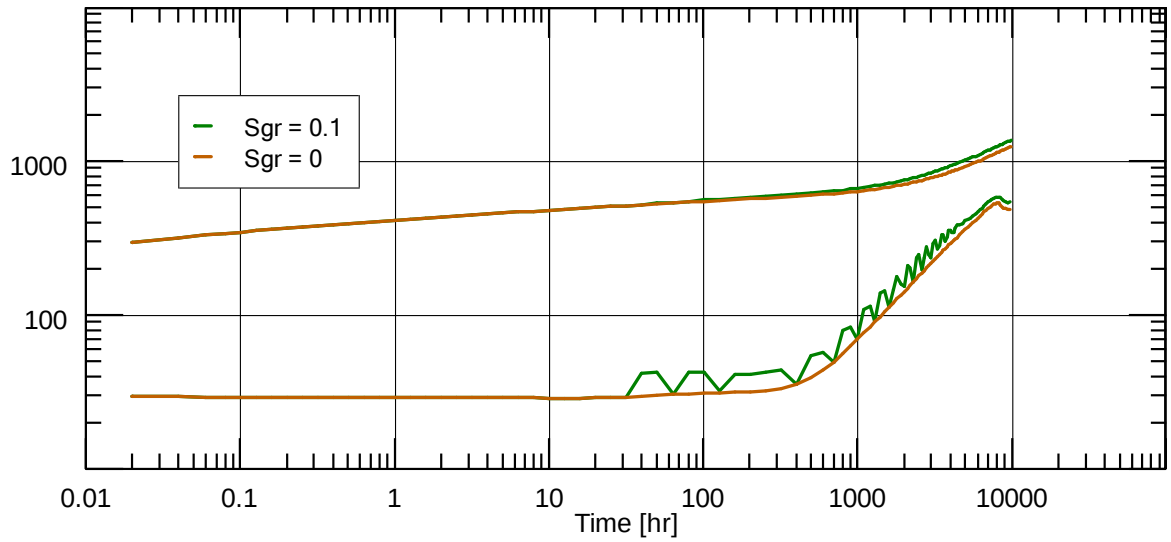

Figure 20: Influence of Sgr on oscillations during production phase (R=50,000 ft, k=100 mD)

3.3. Analysis of multiphase processes during drawdowns and build ups

Drawdown analysis

Figure 21 shows the evolution of the pressure derivative during the production when R=50,000 ft, for three different values of the permeability. Although oscillations are present, we can observe a global increase of the derivative during the depletion. This corresponds to a decrease of the total mobility while gas saturation appears and increases in the reservoir.

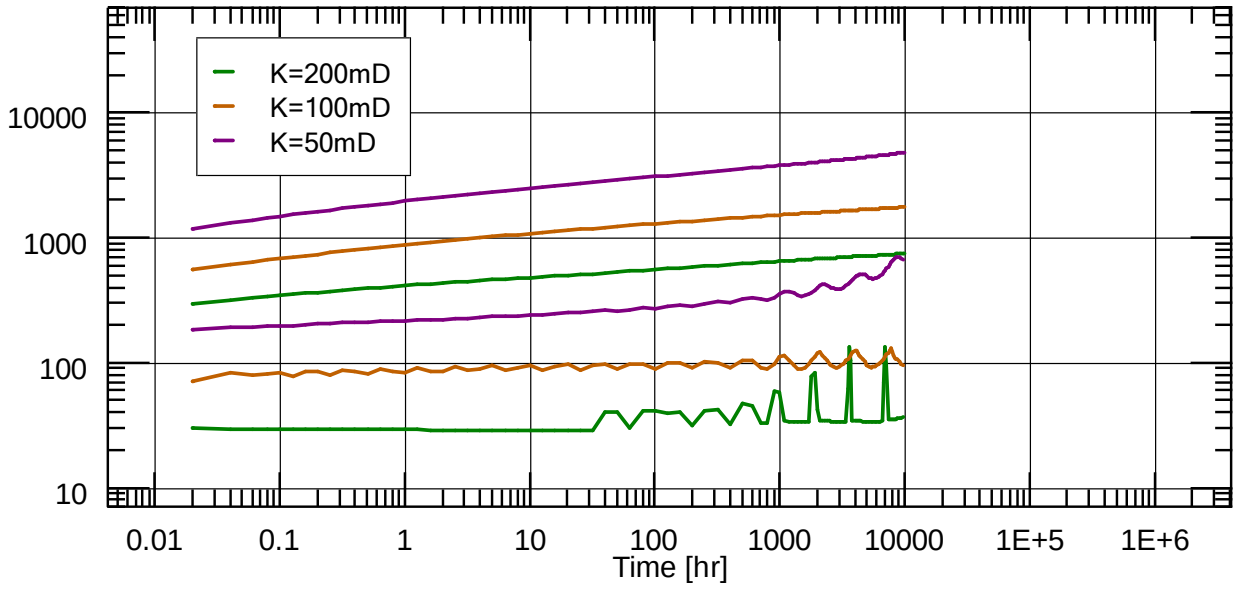

Figure *21: Evolution of the pressure derivative during production phase (R=50,000ft)*

This is partly explained by the non-linearity of the total mobility curve, as previously explained in section 1.2. When gas appears in the medium, the total mobility decreases until the gas saturation reaches a certain value. Note that if one assumes constant viscosities, the mobility decrease is entirely due to the decrease of the relative permeabilities when gas appears in the medium (figure 22).

On Figure 21, however, a significant part of the mobility decrease is also linked to the increase of the oil viscosity when pressure drops below Pb. In particular, the (non-linear) viscosity increase is mainly responsible for the bending trend of the k=50 mD derivative.

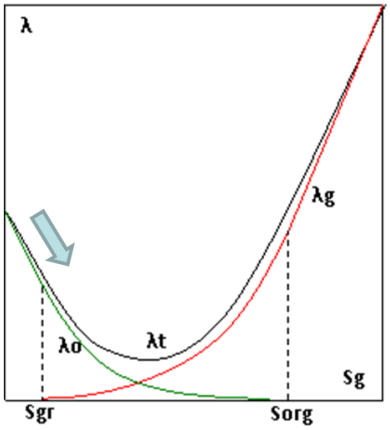

Figure *22: Effect of gas apparition on the total mobility, for constant μ*

Let us now consider a larger depletion, with R=5,000 ft and k=500 mD (Figure 23). The loglog plot derivative can be easily interpreted. The pseudo permanent behavior is reached quickly, around t=50 h, and displays a unit slope until the bubble point is reached, at the well first (at approximately t=1200 hr) but soon everywhere (boundaries reached around t=2,500 hr). This gas apparition is followed by a numerical oscillation. Once gas is present everywhere, the depletion model at constant compressibility (slope 1) hence becomes a model with increasing compressibility. If we assume that the compressibility is proportional to the gas saturation, which is almost proportional to ΔP, the derivative should continue to increase with a slope ½, as confirmed by the simulation result.

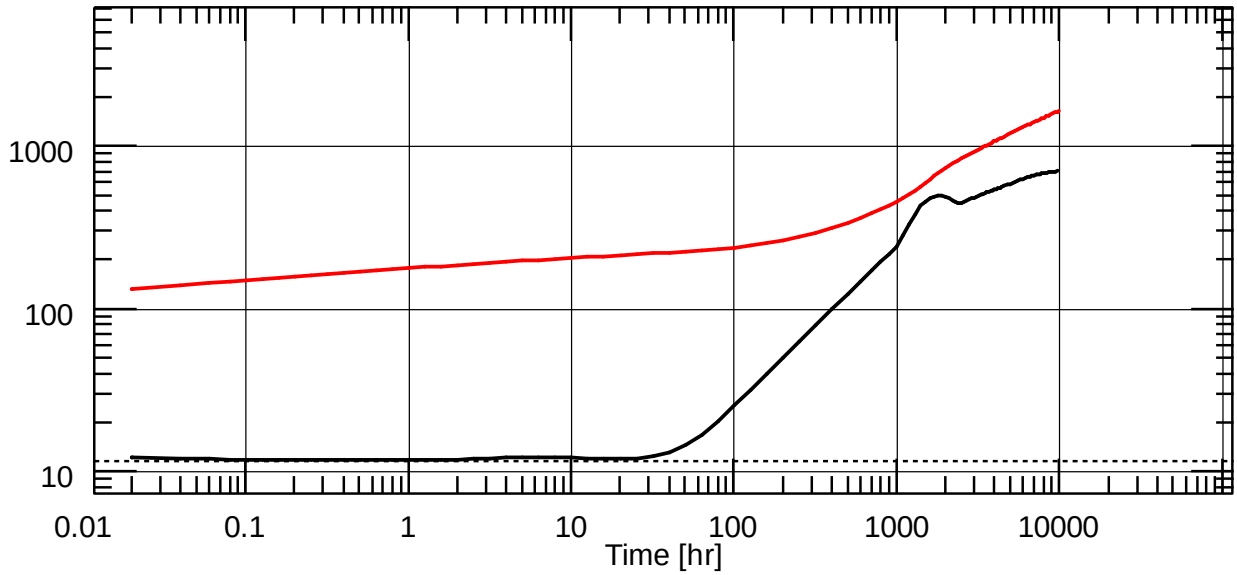

Figure *23: Production phase for R=5,000 ft, k=500 mD*

If the permeability is decreased to k=100 mD (large depletion) a new regime becomes apparent, with a decrease of the derivative level (right of Figure 24). This corresponds to the presence of mobile gas everywhere, with higher saturations compared to the k=500 mD case. As a consequence, the total mobility increases in the medium, as could be predicted from the right side of Figure 22.

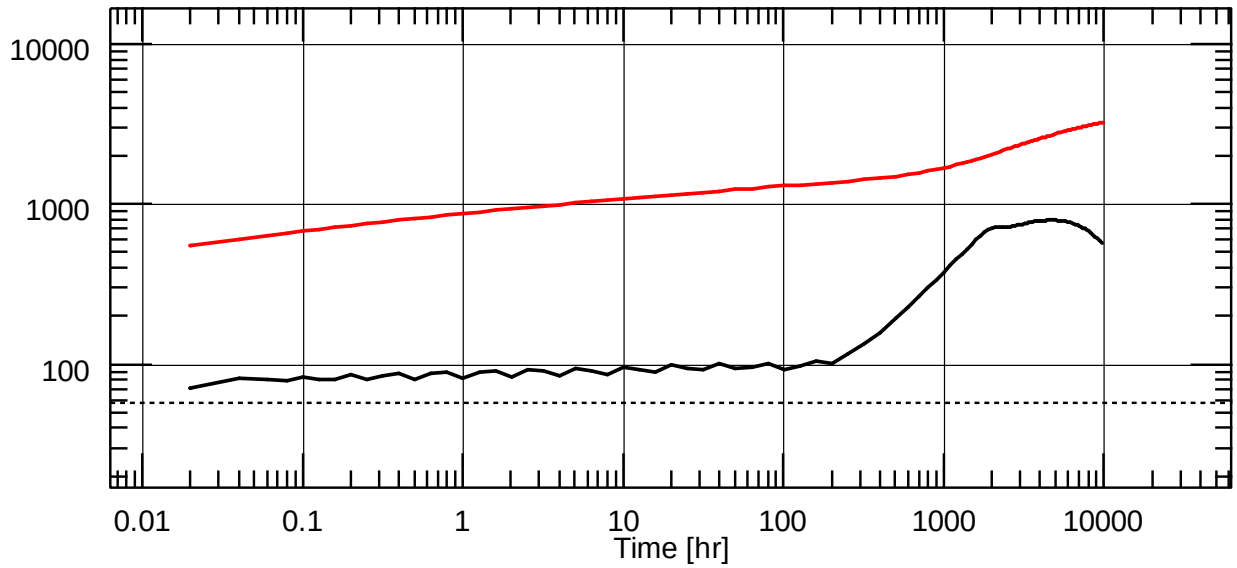

Figure *24: Production phase for R=5,000 ft, k=100 mD*

GOR Analysis

We have seen that although the loglog plot exhibits some oscillations during the production phase, its global trend can be interpreted in terms of fluid mobility. Let us now focus on the evolution of the produced GOR.
For mild depletion (R=50,000 ft, k=100 mD), we have seen that the expansion of the gas bubble in the vicinity of the well was leading to strong oscillations on the pressure derivatives (Figure 18). These oscillations also appear on the GOR, as shown on Figure 25. This is a direct consequence of the transient nature of the flowing composition downstream of a saturation front cell, as was explained in section 3.2 (Figure 19). Note that the vertical scale was greatly increased in order to magnify this effect on Figure 25.

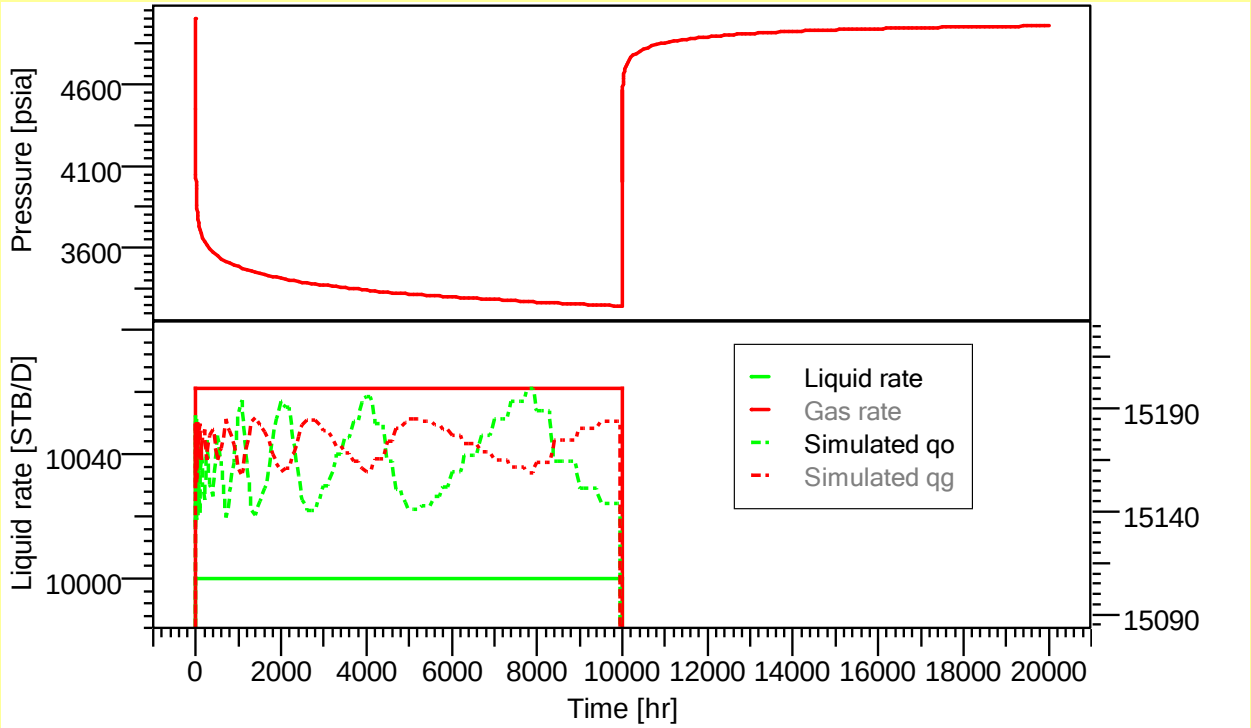

Figure 25*: Evolution of the rates during production phase (R=50,000 ft, k=100 mD)*

Let us consider a slightly stronger depletion, such that gas appears in a wider zone, but with low saturations, so that all the gas is still immobile. This is the case for R=10,000 ft, k=200 mD, as shown on Figure 26. In this case, while the regime becomes pseudo-permanent, the flowing composition becomes representative of the "external" oil depleted at the current external pressure. As a consequence, the produced GOR decreases.

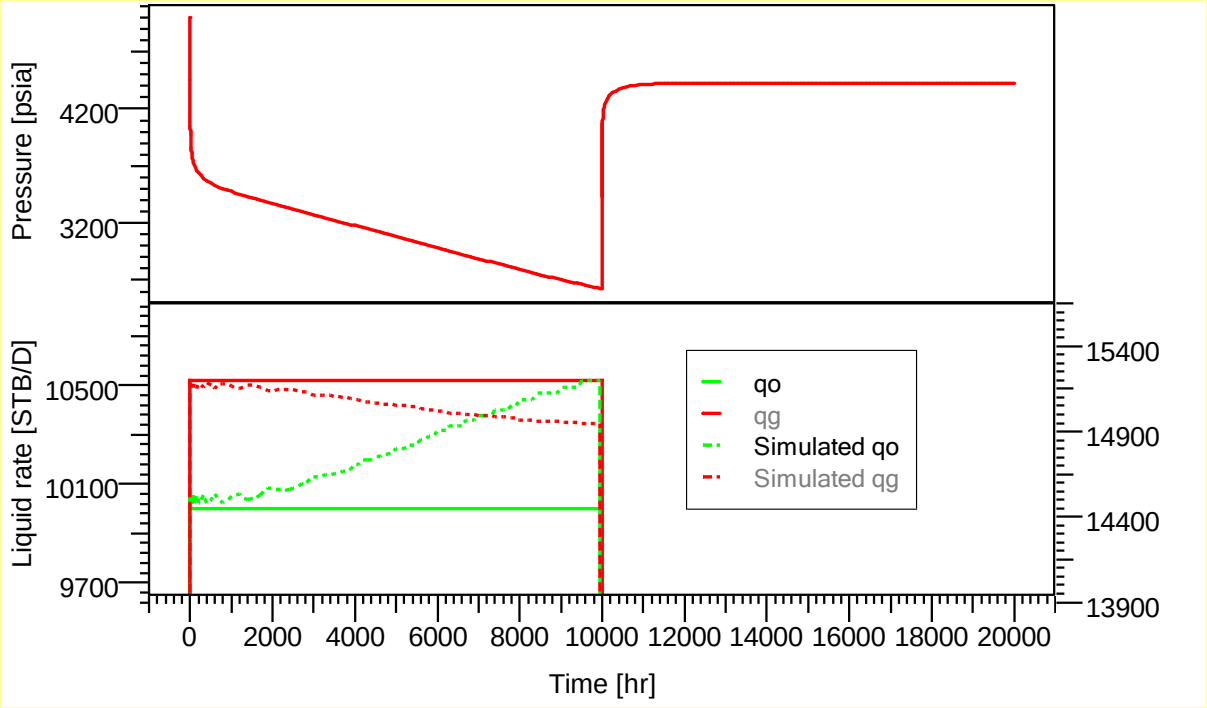

Figure 26*: Evolution of the rates during production phase (R=10,000 ft, k=200mD)*

For a stronger depletion (R=5,000 ft, k=100 mD), the GOR still exhibits a first decrease while the flowing composition stabilizes. Then, the gas saturation increases everywhere, until the gas becomes moveable and starts to be produced. As a consequence, the GOR starts to increase (Figure 27).

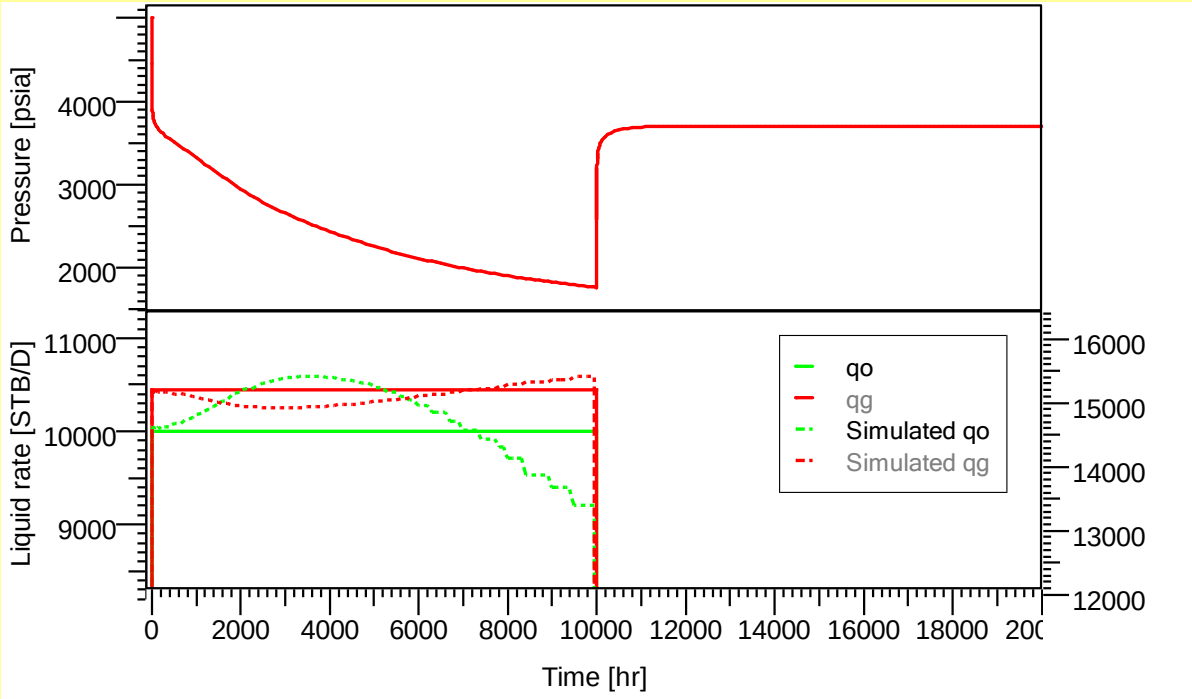

Figure 27*: Evolution of the rates during production phase (R=5,000 ft, k=100 mD)*

Build-up analysis

During the build-up phase, the "gas front" quickly stops progressing. As a consequence, almost no oscillation is visible on loglog build-up derivatives.

The build-up derivative exhibits a transition from the near-well 2-phase region toward the external single phase region, representative of the oil mobility. On Figure 28 (R=50,000 ft, k=100 mD), the inner region shows reduced mobility, because the gas saturation is low, so the total (gas+oil) mobility is lower, as predicted from figure 22.

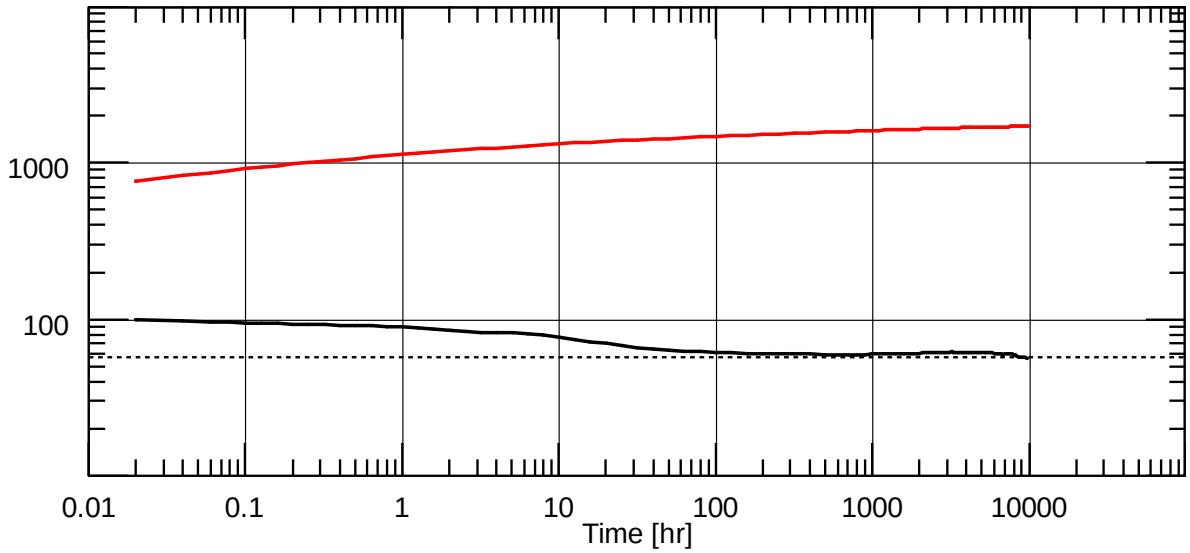

Figure 28: Transition toward single-phase mobility during build-up (R=50,000 ft, k=100 mD)

Evolution of the saturation field during drawdown and build-up

Looking at the gas saturation map at the end of the production phase, Figure 29, we see (as expected) that the saturation decreases while moving away from the well. It is worth mentioning again that due to the stabilization of the flowing composition, the saturations obtained close to the well are higher than what would be obtained from a direct flash of the initial oil at the local pressure.

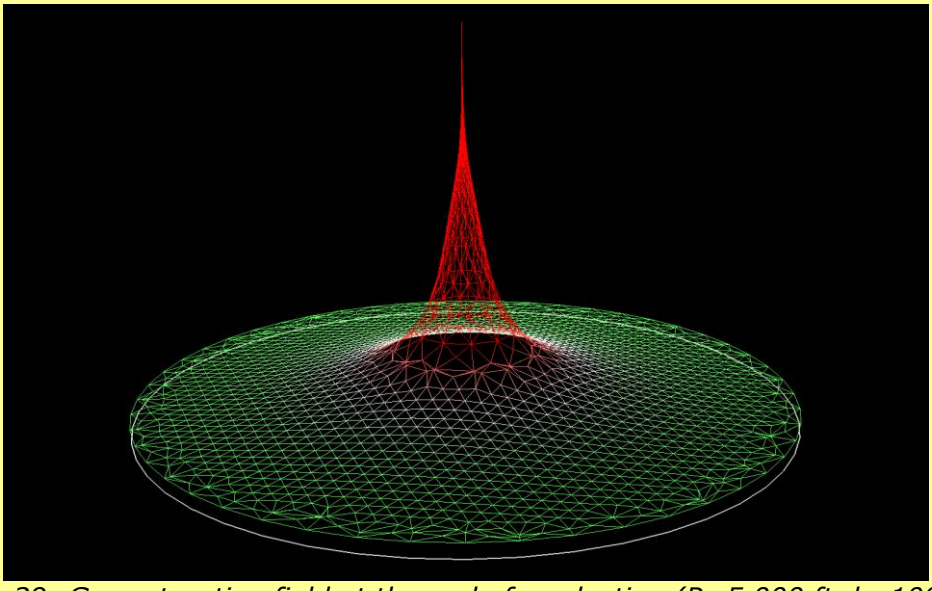

Figure 29: Gas saturation field at the end of production (R=5,000 ft, k=100 mD)

In the immediate vicinity of the well, the oil is very undersaturated. Moreover, during the build-up process, the corresponding cells are further fed with undersaturated oil coming from external cells. As a consequence, while pressure builds up, all the gas can dissolve into oil and the gas saturation decreases to zero in this area (Figure 30).

However, a less intuitive effect is also visible on this figure: an intermediate zone appears where gas is still present at the end of the build-up phase. This is explained by the fact that the global composition in this area was enriched in gas component during the production, as developed below.

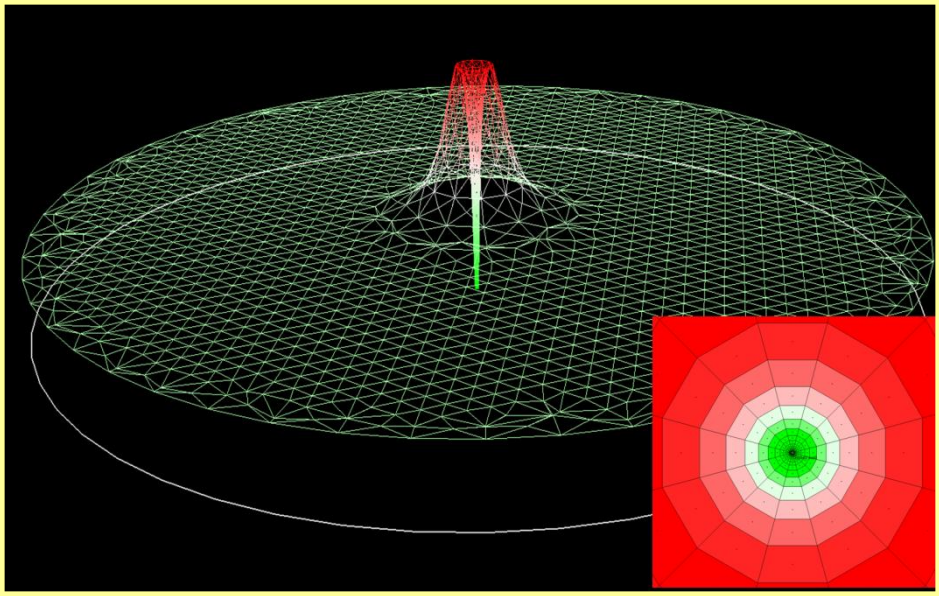

Figure 30: Gas saturation field at the end of build-up (R=5,000ft, k=100mD)

In order to understand this process, let us first consider a constant mass depletion process (Figure 31). Point A corresponds to the composition of the original oil in place at the initial pressure. As the oil is depleted to the local pressure (corresponding to the pressure at the end of the production phase), gas appears if the final pressure is below Pb. Oil and gas are then present in the zone, represented by points D and C. If the pressure comes back to the initial one during the build-up, all the gas should disappear (back to point A on the graph).

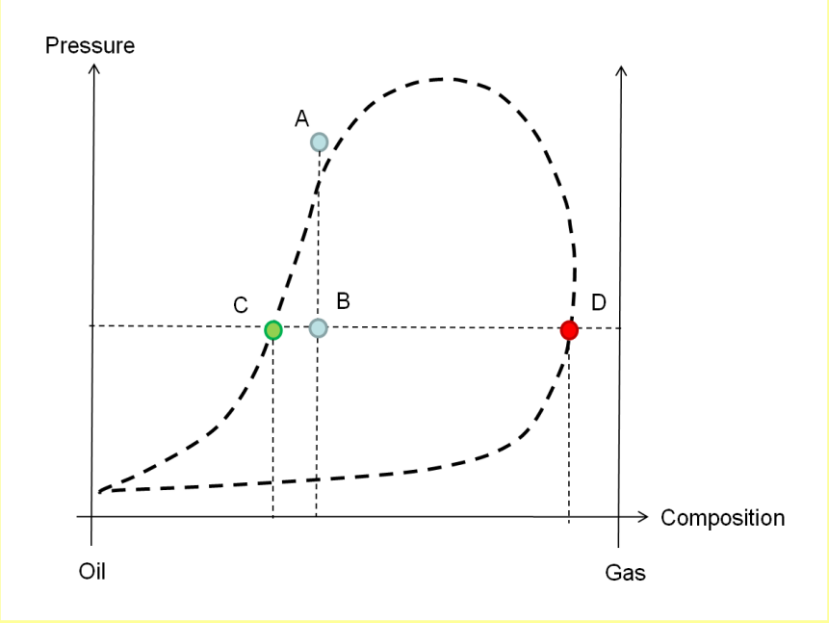

Figure 31: Pressure-composition diagram

In the real production process, however, the depletion does not correspond to a constant mass process, and the global composition in this area was enriched in gas, as represented by point B' on figure 32. When recompressed during the build-up (E), this new composition is still below the bubble point, so gas remains present in the system (points F and G), even if the final pressure is only slightly below the initial one.

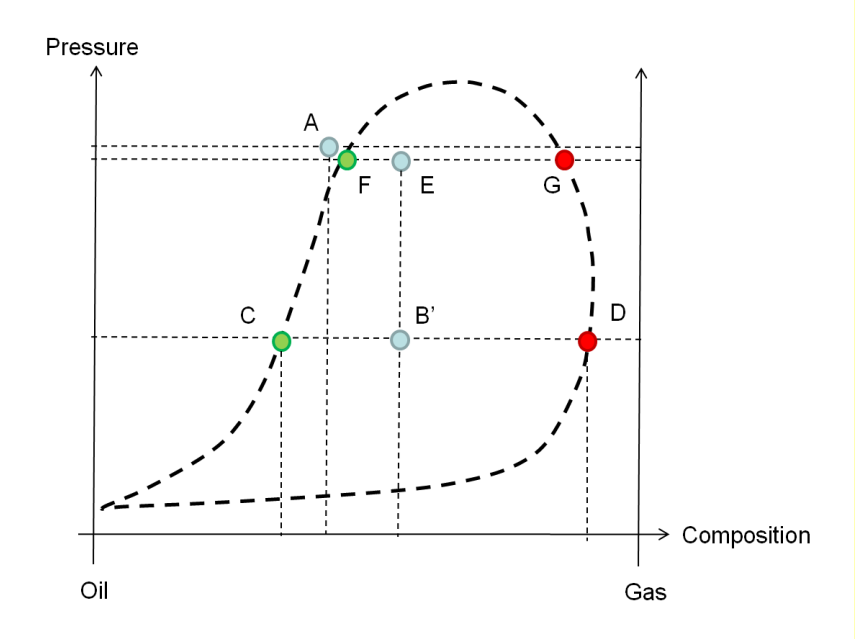

Figure 32: Pressure-composition diagram

3.4. Conclusions for black-oil production

The production of black-oil can be simulated in transient mode using the numerical model in Saphir NL, with some specific observable behavior:

- During the production, pressure can drop below the bubble point and gas can appear in the reservoir. The progression of the gas zone while pressure drops down leads to oscillations on the pressure derivative.
- These oscillations are a consequence of the discretization, and can be significantly damped by reducing the gridding progression ratio. In this case, no correction based on pseudo-kr is possible, because the saturation of gas cannot be related to an actual front position.
- Oscillations do not prevent the interpretation of the loglog plot. In particular, it is possible to relate the observable decrease of mobility to the apparition of gas. Depending on the depletion level, Sgr, etc… several regimes can be identified: a pseudo-steady state regime, a regime with increasing compressibility, corresponding to the increase of gas saturation in the medium, and a regime with higher mobility, corresponding to the flow of mobile gas everywhere.
- Build ups do not exhibit oscillation, and can be interpreted in terms of gas and oil mobilities.
- Finally, many complex processes can be analyzed by examining the evolution of the GOR or of saturation maps. Complete analysis of these multiphase effects is only possible through the use of a non-linear, numerical model.

4. Condensate gas production

We now analyze multiphase effects in the case of condensate gas production. In this situation, mass transfer exists between the two phases, since the heavy component initially present in the rich gas can condensate during depletion, when the pressure drops below the dew point.

4.1. Test Case 4

Test description

The reservoir is circular, with a central well. No water phase is considered. The initial pressure is Pi=5,000 psi. The porosity is Φ = 0.20 and the rock compressibility is cr=3e-6 psi^{-1}.
The gas fluid is defined using the "Condensate (Dew point fluid)" option, using T=300 °F and GOR = 3500 scf/stb at first stage (500 psi, 90 °F), with Pd=4500 psi. Gas gravity is 0.65. All other data are kept at their default values. The resulting maximum liquid deposit is 7.9% at 3140 psi. The Bg curve is fitted with Bg=0.00451 cf/Scf at Pi, while the viscosity curve is fitted at μg=0.053 cp at Pi. The production history is:

- Production for 10,000 hr: Qg=10,000 Mscf/D.
- Build-up for 10,000 hr.

The relative permeability curves are of power-law type with exponent 2, using Sorg =0.25, Sgr=0.05, Krogmax=0.8 and Krgomax=0.5.
In order to investigate different levels of depletion, we ran about 20 simulations on this case, varying both the reservoir radius R (from 5,000 ft to 50,000 ft) and the reservoir permeability k (from 8 mD to 50 mD).

Results

Figure 33 presents the loglog obtained for mild depletion (R=50,000 ft, k=20 mD). The dew point is reached around the well after 16hr of production. Large oscillations are visible as soon as oil appears in the system, not only on the derivative, but also on the pressure curve. As the depletion is limited, the oil deposit extends only in a few cell rings around the well.
Because the process leading to oscillations is the same as for black-oil, previous observations made for black-oil remain true (figures 33 and 34):

- reducing the gridding progression ratio reduces the oscillations level, while increasing their frequency.
- the Sor value also has a great influence on oscillations

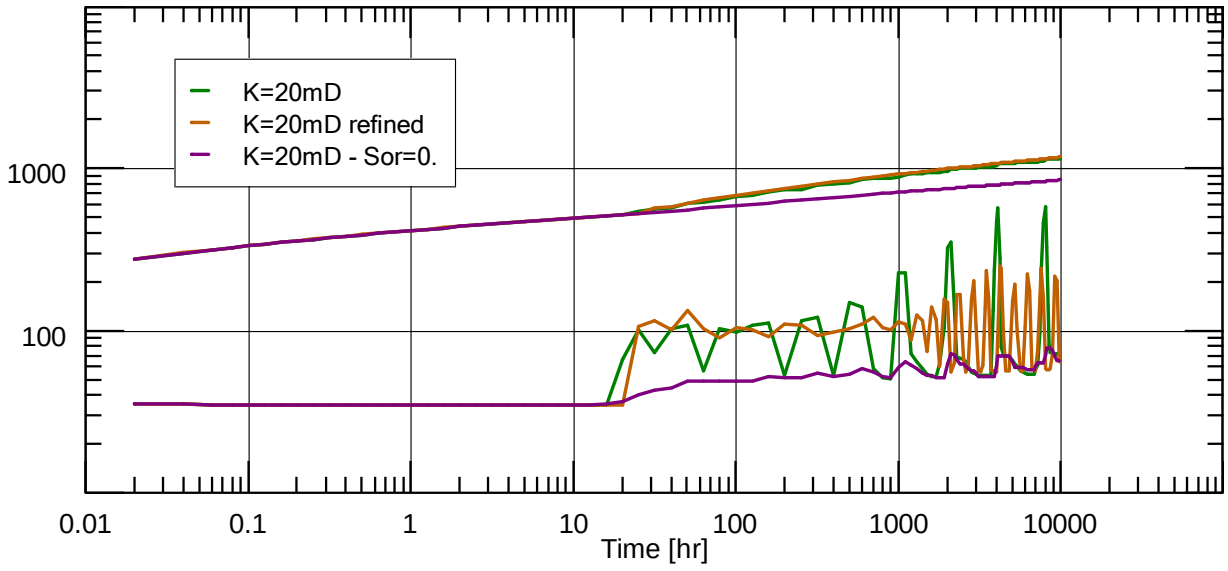

Figure 33: Influence of grid refinement and Sor on oscillations (R=50,000 ft, k=20 mD)

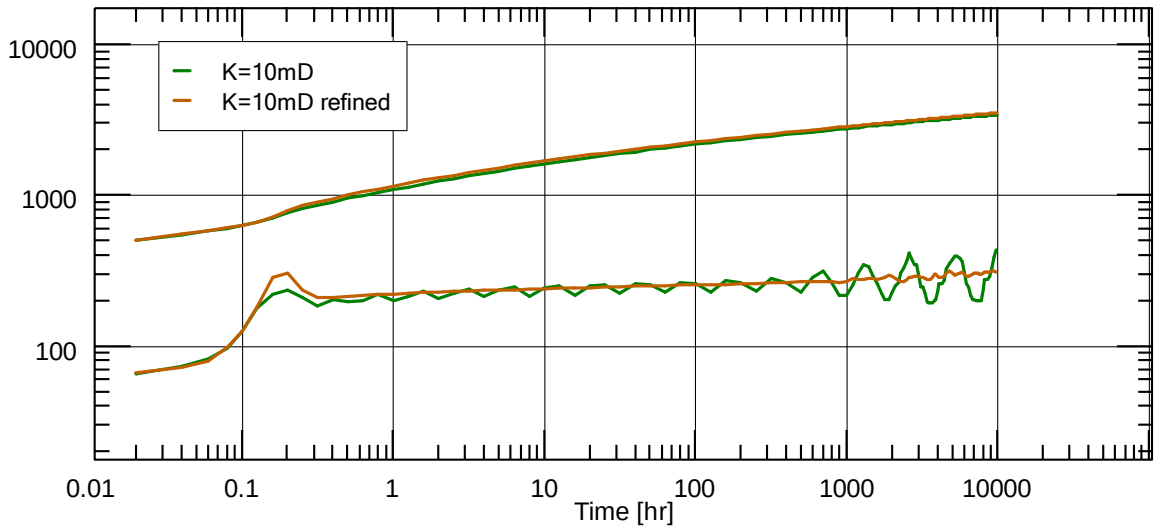

Figure 34: Influence of grid refinement on oscillations (R=50,000 ft, k=10 mD)

4.2. Analysis of multiphase processes during drawdown and build up

Drawdown analysis

Figure 35 shows the evolution of the pressure derivative during the production phase when R=50,000 ft, for three different permeability values. Although oscillations are present, we can observe a global increase of the derivative for each case. This corresponds to a decrease of the total mobility while oil saturation appears and increases in the reservoir.

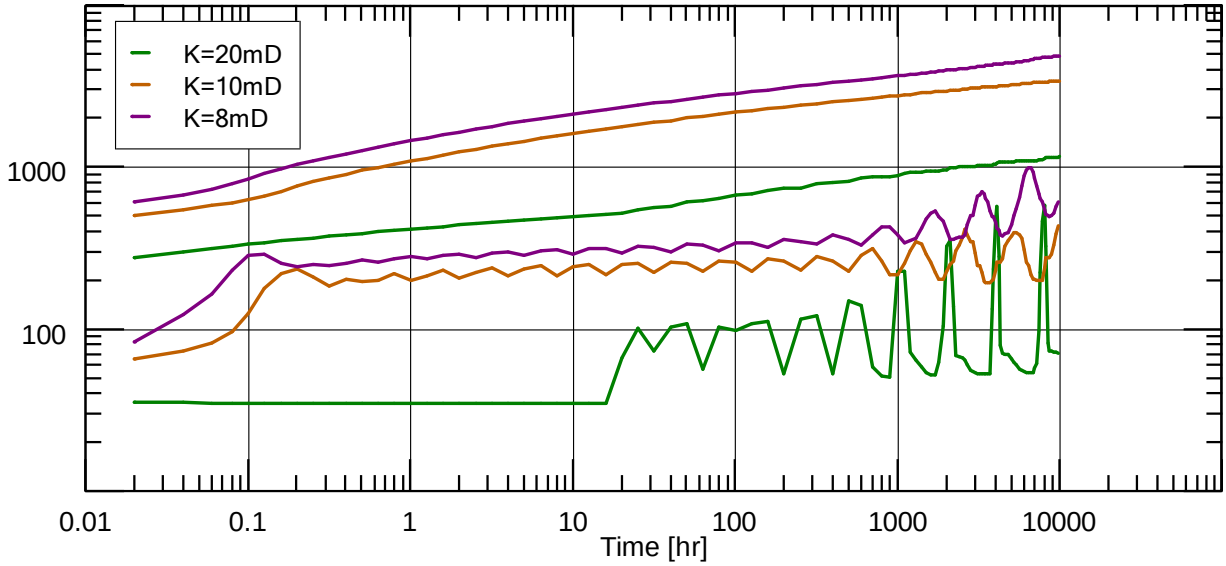

Figure 35: Evolution of the pressure derivative for various values of permeability (R=50,000 ft)

This is explained by the non-linearity of the total mobility curve, as previously explained in section 1.2. When oil appears in the medium, the total mobility decreases as long as the oil saturation is not too high (Figure 36).

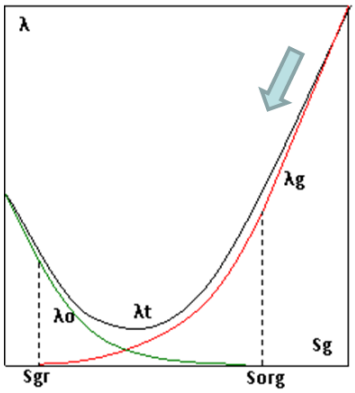

Figure 36: Effect of condensate oil apparition on the total mobility, for constant μ

Let us now consider larger depletions, with R=5,000 ft (Figure 37). In the case k=40 mD, the initial gas reached the dew point around the well at 1120 hr and at the boundaries around 2,500 hr. On this simulation, the derivative curve of the production period can be easily interpreted: the pseudo permanent regime is reached around 100 h, and displays a unit slope until the dew point is reached, at the well first, but soon everywhere. Gas apparition in the medium introduces a single, strong oscillation.

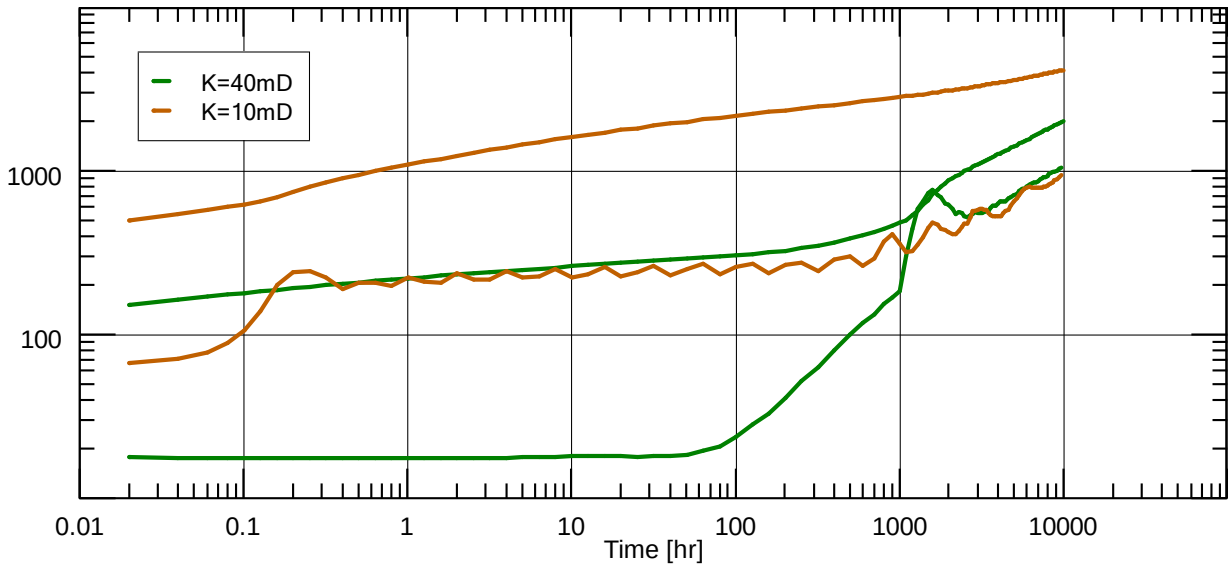

Figure 37: Evolution of the pressure derivative for various values of permeability (R=5,000 ft)

Build-up analysis

During the build-up phase, the "condensate front" quickly stops progressing. As a consequence, almost no oscillation is visible on build-up derivatives, except for some precision-related random noise at late time, as explained below.

The build-up derivative exhibits a transition from the near-well two-phase region toward the external single phase region representative of the gas mobility. On Figure 38 (R=50,000ft, k=10 mD), the inner region shows reduced mobility, because the total (gas+oil) mobility is lower than the single-phase gas mobility.

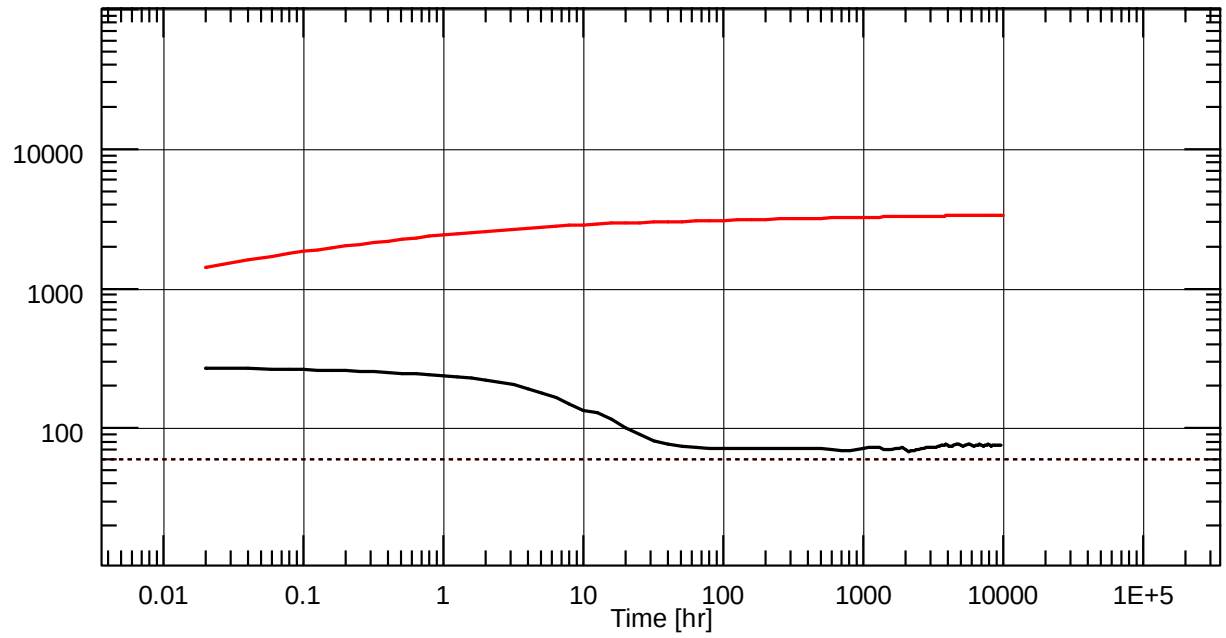

Figure 38: Transition toward single-phase mobility during build-up (R=50,000ft, k=10mD). Late time noise is due to numerical precision

Finally, after 1000 hr, some random noise is visible on the build-up loglog derivative (right part of Figure 38). This noise is due to numerical precision. Indeed, as the reservoir state becomes stable, the well pressure stabilizes around its final value, within a given numerical precision. This precision error leads to small visible derivative changes in this case, as explained at the end of section 2.4. Note that the noise appears at unrealistic late time, when the pressure field is fully stabilized, and that increasing the numerical precision made it disappear.

Evolution of the saturation field during drawdown and build-up

Looking at the oil saturation field at the end of a production phase, we observe an expected bell-shaped condensate zone in the region where P has decreased below Pd (Figure 39).

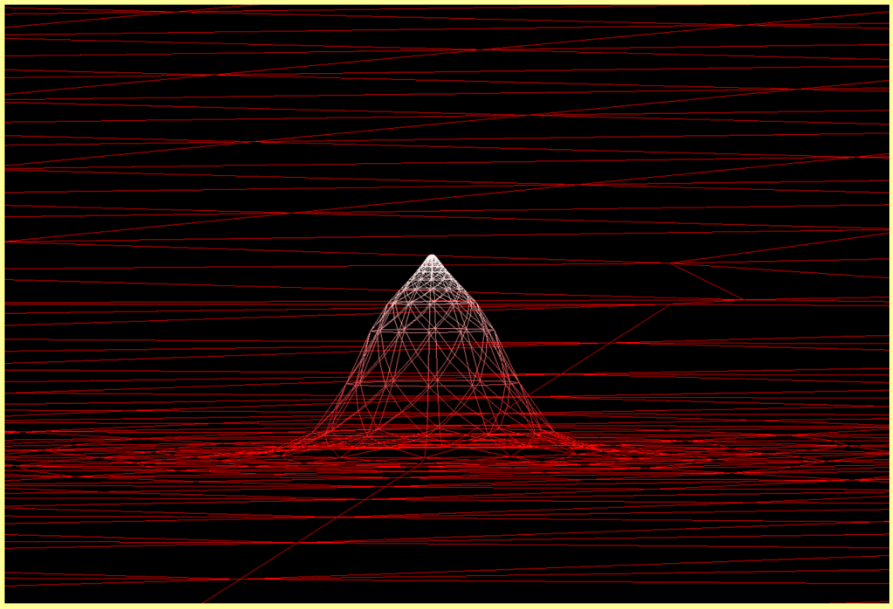

Figure 39: Oil saturation field at the end of the production (R=50,000 ft, k=20 mD)

During the build-up, however, a rather non-intuitive behavior can occur, as shown on Figure 40. In this case, the oil saturation in the immediate vicinity of the well increased, and even reached So=1 at the end of the build-up. This is explained by the fact that the global composition in this area was enriched in heavy component during the production, as developed below.

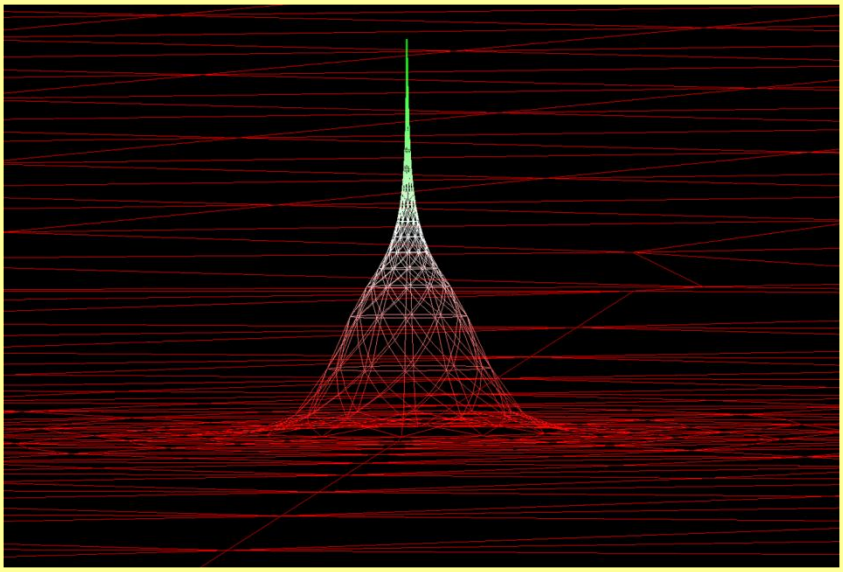

Figure 40: Oil saturation field at the end of the buildup (R=50,000 ft, k=20 mD)

In order to understand this process, let us first consider a constant mass depletion process (Figure 41). Point A corresponds to the composition of the original gas in place at the initial pressure. As the gas is depleted to the local pressure (corresponding to the end of the production phase), an oil condensate appears if the final pressure is below Pd. Oil and gas are then present in the zone, represented by points C and D. If the pressure comes back to the initial one during the buildup, all the oil condensate should vaporize (back to point A on the graph).

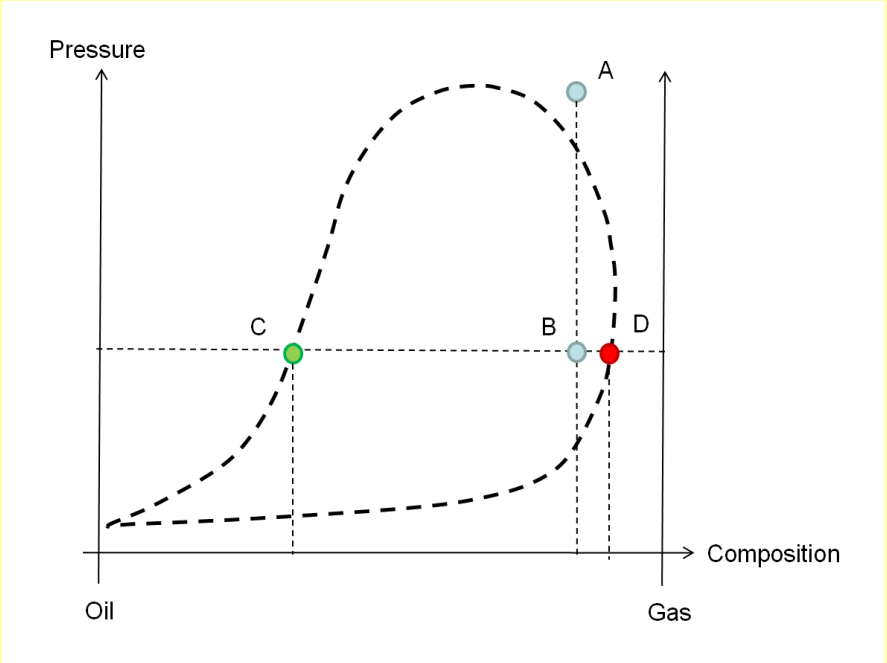

Figure 41: Pressure-composition diagram

In the real production process, however, the global composition in this area was enriched in heavy component, as represented by point B' on figure 42. When recompressed during the build-up, this new composition does not cross the dew pressure curve anymore, but the bubble pressure curve. As a consequence, the free gas obtained at the end of the production process (D) may ultimately dissolve into the oil (point E').

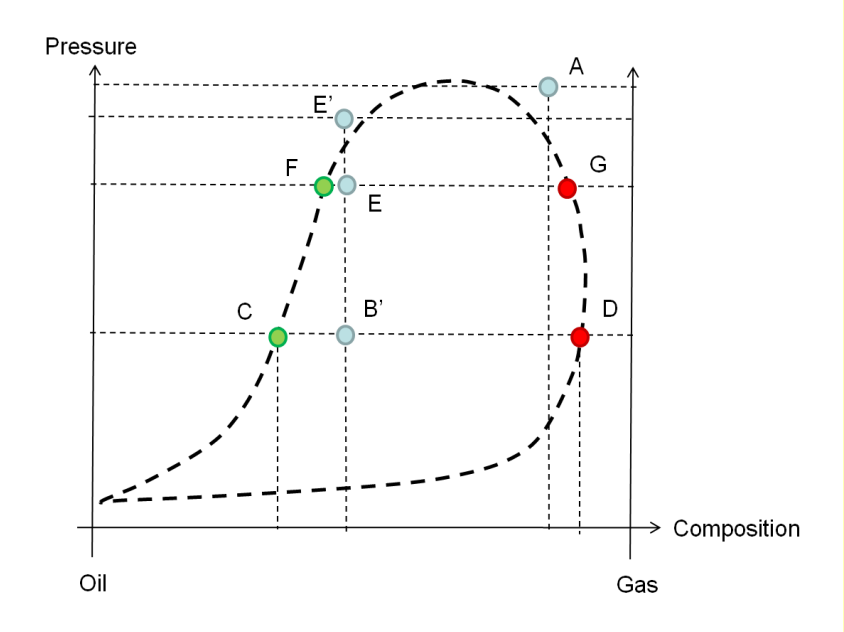

Figure 42: Pressure-composition diagram

4.3. Conclusions for condensate gas production

The production of condensate gas can be simulated in transient mode using the numerical model in Saphir, with some specific observable behavior:

- During the production, pressure can drop below the dew point and an oil condensate can appear in the reservoir. The progression of the condensate zone while pressure drops down leads to strong oscillations on the pressure derivative. These oscillations are a consequence of the discretization, and can be significantly damped by reducing the gridding progression ratio. In this case, no correction based on pseudo-kr is possible, because the condensate saturation cannot be related to an actual front position.
- Oscillations do not prevent the interpretation of the loglog plot. In particular, it is possible to relate the observable decrease of mobility to the apparition of oil.
- Build ups do not exhibit oscillation, and can be interpreted in terms of gas and oil mobilities
- Finally, several complex flow and PVT processes can be analyzed by examining the evolution of the saturation maps. Such analysis is only possible through the use of a non-linear, numerical model.

5. General Conclusions

The discretization process in presence of a moving mobility shock is responsible for visible oscillations on the loglog derivative when analyzing production or injection with multiphase flow. The origin of these oscillations can be rigorously explained.

During water injection, pseudo relative permeability curves are used to correct this phenomenon. For black-oil or condensate gas production curves, refining the grid becomes necessary in order to damp the oscillations. In the case of water injection, the numerical interpretation of flooded distances and fluid mobilities with fall-off curves has been validated against analytical models.

During fall-offs or build-ups, almost no oscillation is visible.

Despite these oscillations, the non-linear numerical model provides an efficient way to interpret many complex multiphase effects, including strong mobility changes, varying GOR and saturation maps.

6. References

Barker and Thibeau, *A Critical Review of the Use of Pseudo Relative Permeabilities for Upscaling*, SPE 35491, European 3D Reservoir Modeling Conference, Stavanger, Norway, 1996

Buckley and Leverett, *Mechanism of Fluid Displacement in Sands*, Trans. AIME, 1942

King and Dunayevsky, *Why Waterflood Works: a Linear Stability Analysis*, SPE 19648, SPE Annual Conference and Exhibition, San Antonio, October 1989

Kyte and Berry, *New Pseudo Functions to control Numerical dispersion*, SPE 5105, 1975

Levitan, *Application of Water Injection/Falloff Tests for Reservoir Appraisal: New Analytical Solution Method for Two-Phase Variable Rate Problems*, SPE 77532, SPE Annual Conference and Exhibition, San Antonio, September 2002

Marle, *Multiphase flow in Porous Media*, Technip Editions, 1981